The Astrophysical Journal, 976:8 (15pp), 2024 November 20 https://doi.org/10.3847/1538-4357/ad812f

Search for Joint Multimessenger Signals from Potential Galactic Cosmic-Ray Accelerators with HAWC and IceCube

R. Alfaro[1], C. Alvarez[2], J. C. Arteaga-Velázquez[3], D. Avila Rojas[1], H. A. Ayala Solares[4], R. Babu[5], E. Belmont-Moreno[1], K. S. Caballero-Mora[2], T. Capistrán[6], A. Carramiñana[7], S. Casanova[8], U. Cotti[3], J. Cotzomi[9], S. Coutiño de León[10], E. De la Fuente[11], D. Depaoli[12], N. Di Lalla[13], R. Diaz Hernandez[7], J. C. Díaz-Vélez[10], K. Engel[14], T. Ergin[5], K. L. Fan[14], K. Fang[10], N. Fraija[6], S. Fraija[6], J. A. García-González[15], F. Garfias[6], M. M. González[6], J. A. Goodman[14], S. Groetsch[16], J. P. Harding[17], S. Hernández-Cadena[18], I. Herzog[5], D. Huang[14], F. Hueyotl-Zahuantitla[2], P. Hüntemeyer[16], A. Iriarte[6], S. Kaufmann[19], J. Lee[20], H. León Vargas[1,7], G. Luis-Raya[19], K. Malone[17], J. Martínez-Castro[21], J. A. Matthews[22], P. Miranda-Romagnoli[23], J. A. Montes[6], E. Moreno[9], M. Mostafá[24], L. Nellen[25], M. U. Nisa[5], N. Omodei[13], M. Osorio[6], Y. Pérez Araujo[6], E. G. Pérez-Pérez[19], C. D. Rho[26], D. Rosa-González[7], H. Salazar[9], D. Salazar-Gallegos[5], A. Sandoval[1], M. Schneider[14], J. Serna-Franco[1], A. J. Smith[14], Y. Son[20], O. Tibolla[19], K. Tollefson[5], I. Torres[7], R. Torres-Escobedo[18], R. Turner[16], F. Ureña-Mena[7], X. Wang[16], I. J. Watson[20], K. Whitaker[4], E. Willox[14], H. Wu[10], S. Yu[4], S. Yun-Cárcamo[14], H. Zhou[18], C. de León[3]
HAWC Collaboration,
and
R. Abbasi[27], M. Ackermann[28], J. Adams[29], S. K. Agarwalla[10,87], J. A. Aguilar[30], M. Ahlers[31], J. M. Alameddine[32], N. M. Amin[33], K. Andeen[34], C. Argüelles[35], Y. Ashida[36], S. Athanasiadou[28], L. Ausborm[37], S. N. Axani[33], X. Bai[38], A. Balagopal V.[10], M. Baricevic[10], S. W. Barwick[39], S. Bash[40], V. Basu[10], R. Bay[41], J. J. Beatty[42,43], J. Becker Tjus[44,88], J. Beise[45], C. Bellenghi[40], C. Benning[37], S. BenZvi[46], D. Berley[14], E. Bernardini[47], D. Z. Besson[48], E. Blaufuss[14], L. Bloom[49], S. Blot[28], F. Bontempo[50], J. Y. Book Motzkin[35], C. Boscolo Meneguolo[47], S. Böser[51], O. Botner[45], J. Böttcher[37], J. Braun[10], B. Brinson[52], J. Brostean-Kaiser[28], L. Brusa[37], R. T. Burley[53], D. Butterfield[10], M. A. Campana[54], I. Caracas[51], K. Carloni[35], J. Carpio[55,56], S. Chattopadhyay[10,87], N. Chau[30], Z. Chen[57], D. Chirkin[10], S. Choi[26,58], B. A. Clark[14], A. Coleman[45], G. H. Collin[59], A. Connolly[42,43], J. M. Conrad[59], P. Coppin[60], R. Corley[36], P. Correa[60], D. F. Cowen[4,61], P. Dave[52], C. De Clercq[60], J. J. DeLaunay[49], D. Delgado[35], S. Deng[37], A. Desai[10], P. Desiati[10], K. D. de Vries[60], G. de Wasseige[62], T. DeYoung[5], A. Diaz[59], P. Dierichs[37], M. Dittmer[63], A. Domi[64], L. Draper[36], H. Dujmovic[10], K. Dutta[51], M. A. DuVernois[10], T. Ehrhardt[51], L. Eidenschink[40], A. Eimer[64], P. Eller[40], E. Ellinger[65], S. El Mentawi[37], D. Elsässer[32], R. Engel[50,66], H. Erpenbeck[10], J. Evans[14], P. A. Evenson[33], K. Farrag[67], A. R. Fazely[68], A. Fedynitch[69], N. Feigl[70], S. Fiedlschuster[64], C. Finley[71], L. Fischer[28], D. Fox[61], A. Franckowiak[44], S. Fukami[28], P. Fürst[37], J. Gallagher[72], E. Ganster[37], A. Garcia[35], M. Garcia[33], G. Garg[10,87], E. Genton[35,62], L. Gerhardt[73], A. Ghadimi[49], C. Girard-Carillo[51], C. Glaser[45], T. Glüsenkamp[45,64], J. G. Gonzalez[33], S. Goswami[55,56], A. Granados[5], D. Grant[5], S. J. Gray[14], O. Gries[37], S. Griffin[10], S. Griswold[46], K. M. Groth[31], C. Günther[37], P. Gutjahr[32], C. Ha[74], C. Haack[64], A. Hallgren[45], L. Halve[37], F. Halzen[10], H. Hamdaoui[57], M. Ha Minh[40], M. Handt[37], K. Hanson[10], J. Hardin[59], A. A. Harnisch[5], P. Hatch[75], A. Haungs[50], J. Häußler[37], K. Helbing[65], J. Hellrung[44], J. Hermannsgabner[37], L. Heuermann[37], N. Heyer[45], S. Hickford[65], A. Hidvegi[71], C. Hill[67], G. C. Hill[53], K. D. Hoffman[14], S. Hori[10], K. Hoshina[10,89], M. Hostert[35], W. Hou[50], T. Huber[50], K. Hultqvist[71], M. Hünnefeld[32], R. Hussain[10], K. Hymon[32], A. Ishihara[67], W. Iwakiri[67], M. Jacquart[10], O. Janik[64], M. Jansson[71], G. S. Japaridze[76], M. Jeong[36], M. Jin[35], B. J. P. Jones[77], N. Kamp[35], D. Kang[50], W. Kang[26], X. Kang[54], A. Kappes[63], D. Kappesser[51], L. Kardum[32], T. Karg[28], M. Karl[40], A. Karle[10], A. Katil[78], U. Katz[64], M. Kauer[10], J. L. Kelley[10], M. Khanal[36], A. Khatee Zathul[10], A. Kheirandish[55,56], J. Kiryluk[57], S. R. Klein[41,73], A. Kochocki[5], R. Koirala[33], H. Kolanoski[70], T. Kontrimas[40], L. Köpke[51], C. Kopper[64], D. J. Koskinen[31], P. Koundal[33], M. Kovacevich[54], M. Kowalski[28,70], T. Kozynets[31], J. Krishnamoorthi[10,87], K. Kruiswijk[62], E. Krupczak[5], A. Kumar[28], E. Kun[44], N. Kurahashi[54], N. Lad[28], C. Lagunas Gualda[28], M. Lamoureux[62], M. J. Larson[14], S. Latseva[37], F. Lauber[65], J. P. Lazar[62], J. W. Lee[26], K. Leonard DeHolton[4], A. Leszczyńska[33], J. Liao[52], M. Lincetto[44], Y. T. Liu[4], M. Liubarska[78], E. Lohfink[51], C. Love[54], C. J. Lozano Mariscal[63], L. Lu[10], F. Lucarelli[79], W. Luszczak[42,43], Y. Lyu[41,73], J. Madsen[10], E. Magnus[60], K. B. M. Mahn[5], Y. Makino[10], E. Manao[40], S. Mancina[10,47], W. Marie Sainte[10], I. C. Mariş[30], S. Marka[80], Z. Marka[80], M. Marsee[49], I. Martinez-Soler[35], R. Maruyama[81], F. Mayhew[5], F. McNally[82], J. V. Mead[31], K. Meagher[10], S. Mechbal[28], A. Medina[43], M. Meier[67], Y. Merckx[60], L. Merten[44], J. Micallef[5], J. Mitchell[68], T. Montaruli[79], R. W. Moore[78], Y. Morii[67], R. Morse[10], M. Moulai[10], T. Mukherjee[50], R. Naab[28], R. Nagai[67], M. Nakos[10], U. Naumann[65], J. Necker[28], A. Negi[77], L. Neste[71], M. Neumann[63], H. Niederhausen[5], K. Noda[67], A. Noell[37], A. Novikov[33], A. Obertacke Pollmann[67], V. O'Dell[10], B. Oeyen[83], A. Olivas[14], R. Orsoe[40], J. Osborn[10], E. O'Sullivan[45], H. Pandya[33], N. Park[75], G. K. Parker[77], E. N. Paudel[33], L. Paul[38], C. Pérez de los Heros[45], T. Pernice[28], J. Peterson[10], S. Philippen[37], A. Pizzuto[10], M. Plum[38], A. Pontén[45], Y. Popovych[51], M. Prado Rodriguez[10], B. Pries[5], R. Procter-Murphy[14], G. T. Przybylski[73], C. Raab[62], J. Rack-Helleis[51], M. Ravn[45], K. Rawlins[84], Z. Rechav[10], A. Rehman[33], P. Reichherzer[44], E. Resconi[40], S. Reusch[28], W. Rhode[32], B. Riedel[10], A. Rifaie[37], E. J. Roberts[53], S. Robertson[41,73], S. Rodan[26,58], G. Roellinghoff[26], M. Rongen[64],

A. Rosted[67], C. Rott[36,26], T. Ruhe[32], L. Ruohan[40], D. Ryckbosch[83], I. Safa[10], J. Saffer[66], P. Sampathkumar[50], A. Sandrock[65], M. Santander[49], S. Sarkar[78], S. Sarkar[85], J. Savelberg[37], P. Savina[10], P. Schaile[40], M. Schaufel[37], H. Schieler[50], S. Schindler[64], B. Schlüter[63], F. Schlüter[30], N. Schmeisser[65], T. Schmidt[14], J. Schneider[64], F. G. Schröder[33,50], L. Schumacher[64], S. Sclafani[14], D. Seckel[33], M. Seikh[48], M. Seo[26], S. Seunarine[86], P. Sevle Myhr[62], R. Shah[54], S. Shefali[66], N. Shimizu[67], M. Silva[10], B. Skrzypek[41], B. Smithers[77], R. Snihur[10], J. Soedingrekso[32], A. Søgaard[31], D. Soldin[36], P. Soldin[37], G. Sommani[44], C. Spannfellner[40], G. M. Spiczak[86], C. Spiering[28], M. Stamatikos[43], T. Stanev[33], T. Stezelberger[73], T. Stürwald[65], T. Stuttard[31], G. W. Sullivan[14], I. Taboada[52], S. Ter-Antonyan[68], A. Terliuk[40], M. Thiesmeyer[37], W. G. Thompson[35], J. Thwaites[10], S. Tilav[33], C. Tönnis[26], S. Toscano[30], D. Tosi[10], A. Trettin[28], R. Turcotte[50], J. P. Twagirayezu[5], M. A. Unland Elorrieta[63], A. K. Upadhyay[10,87], K. Upshaw[68], A. Vaidyanathan[34], N. Valtonen-Mattila[45], J. Vandenbroucke[10], N. van Eijndhoven[60], D. Vannerom[59], J. van Santen[28], J. Vara[63], J. Veitch-Michaelis[10], M. Venugopal[50], M. Vereecken[62], S. Verpoest[33], D. Veske[80], A. Vijai[14], C. Walck[71], A. Wang[52], C. Weaver[5], P. Weigel[59], A. Weindl[50], J. Weldert[4], A. Y. Wen[35], C. Wendt[10], J. Werthebach[32], M. Weyrauch[50], N. Whitehorn[5], C. H. Wiebusch[37], D. R. Williams[49], L. Witthaus[32], A. Wolf[37], M. Wolf[40], G. Wrede[64], X. W. Xu[68], J. P. Yanez[78], E. Yildizci[10], S. Yoshida[67], R. Young[48], S. Yu[36], T. Yuan[10], Z. Zhang[57], P. Zhelnin[35], P. Zilberman[10], and M. Zimmerman[10]

IceCube Collaboration

[1] Instituto de Física, Universidad Nacional Autónoma de México, Ciudad de Mexico, Mexico; analysis@icecube.wisc.edu
[2] Universidad Autónoma de Chiapas, Tuxtla Gutiérrez, Chiapas, Mexico
[3] Universidad Michoacana de San Nicolás de Hidalgo, Morelia, Mexico
[4] Department of Physics, Pennsylvania State University, University Park, PA 16802, USA
[5] Department of Physics and Astronomy, Michigan State University, East Lansing, MI, USA
[6] Instituto de Astronomía, Universidad Nacional Autónoma de México, Ciudad de Mexico, Mexico
[7] Instituto Nacional de Astrofísica, Óptica y Electrónica, Puebla, Mexico
[8] Institute of Nuclear Physics Polish Academy of Sciences, PL-31342 IFJ-PAN, Krakow, Poland
[9] Facultad de Ciencias Físico Matemáticas, Benemérita Universidad Autónoma de Puebla, Puebla, Mexico
[10] Department of Physics and Wisconsin IceCube Particle Astrophysics Center, University of Wisconsin–Madison, Madison, WI 53706, USA
[11] Departamento de Física, Centro Universitario de Ciencias Exactase Ingenierias, Universidad de Guadalajara, Guadalajara, Mexico
[12] Max-Planck Institute for Nuclear Physics, 69117 Heidelberg, Germany
[13] Department of Physics, Stanford University: Stanford, CA 94305-4060, USA
[14] Department of Physics, University of Maryland, College Park, MD, USA; klfan@umd.edu
[15] Instituto Tecnológico y de Estudios Superiores de Monterrey—Campus Toluca: Toluca de Lerdo, Estado de México, Mexico,
[16] Department of Physics, Michigan Technological University, Houghton, MI, USA
[17] Physics Division, Los Alamos National Laboratory, Los Alamos, NM, USA
[18] Tsung-Dao Lee Institute & School of Physics and Astronomy, Shanghai Jiao Tong University, Shanghai, People's Republic of China
[19] Universidad Politécnica de Pachuca, Pachuca, Hgo, Mexico
[20] Natural Science Research Institute, University of Seoul, Seoul, Republic of Korea
[21] Centro de Investigación en Computación, Instituto Politécnico Nacional, México City, Mexico
[22] Department of Physics and Astronomy, University of New Mexico, Albuquerque, NM, USA
[23] Universidad Autónoma del Estado de Hidalgo, Pachuca, Mexico
[24] Department of Physics, Temple University, Philadelphia, Pennsylvania, USA
[25] Instituto de Ciencias Nucleares, Universidad Nacional Autónoma de Mexico, Ciudad de Mexico, Mexico
[26] Department of Physics, Sungkyunkwan University, Suwon 16419, Republic of Korea
[27] Department of Physics, Loyola University Chicago, Chicago, IL 60660, USA
[28] Deutsches Elektronen-Synchrotron DESY, Platanenallee 6, D-15738 Zeuthen, Germany
[29] Department of Physics and Astronomy, University of Canterbury, Private Bag 4800, Christchurch, New Zealand
[30] Université Libre de Bruxelles, Science Faculty CP230, B-1050 Brussels, Belgium
[31] Niels Bohr Institute, University of Copenhagen, DK-2100 Copenhagen, Denmark
[32] Department of Physics, TU Dortmund University, D-44221 Dortmund, Germany
[33] Bartol Research Institute and Dept. of Physics and Astronomy, University of Delaware, Newark, DE 19716, USA
[34] Department of Physics, Marquette University, Milwaukee, WI 53201, USA
[35] Department of Physics and Laboratory for Particle Physics and Cosmology, Harvard University, Cambridge, MA 02138, USA
[36] Department of Physics and Astronomy, University of Utah, Salt Lake City, UT 84112, USA
[37] III. Physikalisches Institut, RWTH Aachen University, D-52056 Aachen, Germany
[38] Physics Department, South Dakota School of Mines and Technology, Rapid City, SD 57701, USA
[39] Department of Physics and Astronomy, University of California, Irvine, CA 92697, USA
[40] Physik-department, Technische Universität München, D-85748 Garching, Germany
[41] Department of Physics, University of California, Berkeley, CA 94720, USA
[42] Department of Astronomy, Ohio State University, Columbus, OH 43210, USA
[43] Department of Physics and Center for Cosmology and Astro-Particle Physics, Ohio State University, Columbus, OH 43210, USA
[44] Fakultät für Physik & Astronomie, Ruhr-Universität Bochum, D-44780 Bochum, Germany
[45] Department of Physics and Astronomy, Uppsala University, Box 516, SE-75120 Uppsala, Sweden
[46] Department of Physics and Astronomy, University of Rochester, Rochester, NY 14627, USA
[47] Dipartimento di Fisica e Astronomia Galileo Galilei, Università Degli Studi di Padova, I-35122 Padova PD, Italy
[48] Department of Physics and Astronomy, University of Kansas, Lawrence, KS 66045, USA
[49] Department of Physics and Astronomy, University of Alabama, Tuscaloosa, AL 35487, USA
[50] Karlsruhe Institute of Technology, Institute for Astroparticle Physics, D-76021 Karlsruhe, Germany
[51] Institute of Physics, University of Mainz, Staudinger Weg 7, D-55099 Mainz, Germany
[52] School of Physics and Center for Relativistic Astrophysics, Georgia Institute of Technology, Atlanta, GA 30332, USA
[53] Department of Physics, University of Adelaide, Adelaide, 5005, Australia
[54] Department of Physics, Drexel University, 3141 Chestnut Street, Philadelphia, PA 19104, USA
[55] Department of Physics & Astronomy, University of Nevada, Las Vegas, NV 89154, USA

[56] Nevada Center for Astrophysics, University of Nevada, Las Vegas, NV 89154, USA
[57] Dept. of Physics and Astronomy, Stony Brook University, Stony Brook, NY 11794-3800, USA
[58] Institute of Basic Science, Sungkyunkwan University, Suwon 16419, Republic of Korea
[59] Department of Physics, Massachusetts Institute of Technology, Cambridge, MA 02139, USA
[60] Vrije Universiteit Brussel (VUB), Dienst ELEM, B-1050 Brussels, Belgium
[61] Department of Astronomy and Astrophysics, Pennsylvania State University, University Park, PA 16802, USA
[62] Centre for Cosmology, Particle Physics and Phenomenology - CP3, Université catholique de Louvain, Louvain-la-Neuve, Belgium
[63] Institut für Kernphysik, Westfälische Wilhelms-Universität Münster, D-48149 Münster, Germany
[64] Erlangen Centre for Astroparticle Physics, Friedrich-Alexander-Universität Erlangen-Nürnberg, D-91058 Erlangen, Germany
[65] Department of Physics, University of Wuppertal, D-42119 Wuppertal, Germany
[66] Karlsruhe Institute of Technology, Institute of Experimental Particle Physics, D-76021 Karlsruhe, Germany
[67] Department of Physics and The International Center for Hadron Astrophysics, Chiba University, Chiba 263-8522, Japan
[68] Department of Physics, Southern University, Baton Rouge, LA 70813, USA
[69] Institute of Physics, Academia Sinica, Taipei, 11529, Taiwan
[70] Institut für Physik, Humboldt-Universität zu Berlin, D-12489 Berlin, Germany
[71] Oskar Klein Centre and Dept. of Physics, Stockholm University, SE-10691 Stockholm, Sweden
[72] Department of Astronomy, University of Wisconsin–Madison, Madison, WI 53706, USA
[73] Lawrence Berkeley National Laboratory, Berkeley, CA 94720, USA
[74] Department of Physics, Chung-Ang University, Seoul 06974, Republic of Korea
[75] Department of Physics, Engineering Physics, and Astronomy, Queen's University, Kingston, ON K7L 3N6, Canada
[76] CTSPS, Clark-Atlanta University, Atlanta, GA 30314, USA
[77] Dept. of Physics, University of Texas at Arlington, 502 Yates St., Science Hall Rm 108, Box 19059, Arlington, TX 76019, USA
[78] Department of Physics, University of Alberta, Edmonton, Alberta, T6G 2E1, Canada
[79] Département de physique nucléaire et corpusculaire, Université de Genève, CH-1211 Genève, Switzerland
[80] Columbia Astrophysics and Nevis Laboratories, Columbia University, New York, NY 10027, USA
[81] Department of Physics, Yale University, New Haven, CT 06520, USA
[82] Department of Physics, Mercer University, Macon, GA 31207-0001, USA
[83] Department of Physics and Astronomy, University of Gent, B-9000 Gent, Belgium
[84] Department of Physics and Astronomy, University of Alaska Anchorage, 3211 Providence Dr., Anchorage, AK 99508, USA
[85] Department of Physics, University of Oxford, Parks Road, Oxford OX1 3PU, UK
[86] Department of Physics, University of Wisconsin, River Falls, WI 54022, USA
Received 2024 May 6; revised 2024 September 24; accepted 2024 September 26; published 2024 November 11

Abstract

The origin of high-energy galactic cosmic rays is yet to be understood, but some galactic cosmic-ray accelerators can accelerate cosmic rays up to PeV energies. The high-energy cosmic rays are expected to interact with the surrounding material or radiation, resulting in the production of gamma-rays and neutrinos. To optimize for the detection of such associated production of gamma-rays and neutrinos for a given source morphology and spectrum, a multimessenger analysis that combines gamma-rays and neutrinos is required. In this study, we use the Multi-Mission Maximum Likelihood framework with IceCube Maximum Likelihood Analysis software and HAWC Accelerated Likelihood to search for a correlation between 22 known gamma-ray sources from the third HAWC gamma-ray catalog and 14 yr of IceCube track-like data. No significant neutrino emission from the direction of the HAWC sources was found. We report the best-fit gamma-ray model and 90% CL neutrino flux limit from the 22 sources. From the neutrino flux limit, we conclude that, for five of the sources, the gamma-ray emission observed by HAWC cannot be produced purely from hadronic interactions. We report the limit for the fraction of gamma-rays produced by hadronic interactions for these five sources.

Unified Astronomy Thesaurus concepts: Neutrino astronomy (1100); Gamma-ray astronomy (628); Particle astrophysics (96); High energy astrophysics (739)

1. Introduction

Cosmic rays (CRs) were discovered more than 100 yr ago (V. F. Hess 1912), but where these high-energy particles come from has not yet been well understood. The highest-energy charged particles, protons and nuclei, are thought to be extraterrestrial in origin, and their spectrum can be parameterized using a power law with an index of 2.7 up to $E_{\rm CR} \sim 3$ PeV (or the "knee" in the spectrum), above which the spectrum steepens (M. Nagano et al. 1984; M. A. K. Glasmacher et al. 1999; M. Amenomori et al. 2008; R. U. Abbasi et al. 2018; M. G. Aartsen et al. 2020a; Z. Cao et al. 2024a). The CRs below the knee are thought to originate from sources within the Milky Way galaxy, hinting at the presence of PeV hadron accelerators within the galaxy known as Galactic PeVatrons (S. Gabici & F. A. Aharonian 2007). Galactic PeVatrons are expected to accelerate particles up to PeV energies through Fermi acceleration, and these accelerated particles are expected to be confined within the Milky Way galaxy (E. de Oña Wilhelmi et al. 2024). The AS gamma collaboration reported the detection of diffuse gamma-rays from the galactic disk with energy between 100 TeV and 1 PeV, hinting at the presence of PeVatrons within our galaxy (M. Amenomori et al. 2021).

[87] also at Institute of Physics, Sachivalaya Marg, Sainik School Post, Bhubaneswar 751005, India.
[88] also at Department of Space, Earth and Environment, Chalmers University of Technology, 412 96 Gothenburg, Sweden.
[89] also at Earthquake Research Institute, University of Tokyo, Bunkyo, Tokyo 113-0032, Japan.

Supernova remnants (SNRs) are a potential class of Galactic PeVatrons. The particles are accelerated by diffusive shock acceleration in the expanding shock. Only 10% of the energy of SNRs is needed to account for the observed CR energy density in the Galaxy (R. D. Blandford & J. P. Ostriker 1978). For the most energetic galactic CRs, it is assumed that only young SNRs can accelerate CRs beyond 100 TeV (A. R. Bell et al. 2013). The accelerated CRs can escape the SNR and diffuse into the surrounding interstellar medium. They can interact with the surrounding material like molecular clouds and produce charged and neutral pions. Therefore, young SNRs located near star clusters or molecular clouds are thought to be bright in gamma-rays due to hadronic interactions. High-energy gamma-rays and neutrinos can be efficiently produced by the decay of charged and neutral pions. Other potential classes of Galactic PeVatrons include young massive star clusters (YMCs; A. M. Bykov et al. 2020) and pulsar wind nebulae (PWNe; I. Di Palma et al. 2017).

TeV gamma-rays can also be produced by leptonic interactions such as inverse Compton scattering. However, inverse Compton scattering is strongly suppressed at energies above 50 TeV (J. A. Hinton & W. Hofmann 2009) due to the Klein–Nishina effect (O. Klein & T. Nishina 1929). On the other hand, the gamma-rays produced by neutral pion decays are not suppressed at O(10 TeV), making TeV gamma-ray emitters excellent candidates for Galactic PeVatrons. Moreover, high-energy neutrinos are also produced in hadronic interactions via charged pion decays, and their detection is evidence of hadron acceleration. Because of this relationship, a joint search using TeV gamma-ray and neutrino data from known TeV gamma-ray emitters can test whether a source is a Galactic PeVatron.

Several potential Galactic PeVatrons have been investigated by the community. The HAWC collaboration reported that the TeV gamma-ray spectrum of HAWC J1825−134 extends up to 200 TeV without any cutoff, much higher than the Klein–Nishina suppression energy (A. Albert et al. 2021). This may indicate hadronic acceleration. The HAWC collaboration also reported HAWC J2227+610 as a potential PeVatron candidate from TeV gamma-ray observations and concluded the proton cutoff energy is at least 800 TeV (A. Albert et al. 2020a). The HAWC collaboration studied the ultra-high-energy spectrum of MGRO J1908+06, and their model allows a hadronic component at the highest energy (A. Albert et al. 2022). The HESS Collaboration reported evidence of a PeVatron at the Galactic center based on gamma-ray observations up to 40 TeV (A. Abramowski et al. 2016). The LHAASO collaboration reported an ultra-high-energy gamma-ray bubble up to a few PeV from the direction of the Cygnus X region, and suggested that a super PeVatron with maximum proton energy of 10 PeV could power the source (LHAASO Collaboration 2024). The LHAASO collaboration detected 12 gamma-ray sources with emissions above 100 TeV (Z. Cao et al. 2021) and recently reported their first catalog 1LHAASO (Z. Cao et al. 2024b). The 1LHAASO contains 90 gamma-ray sources, and 43 sources have emission above 100 TeV, making them possible Galactic PeVatrons.

Many efforts have been made to search for PeVatrons using neutrino data. T.-Q. Huang & Z. Li (2022a) set a constraint on neutrino emission from LHAASO's first catalog of sources with energy above 100 TeV (Z. Cao et al. 2021) using previous IceCube neutrino upper limits. They used measurements from other gamma-ray instruments and constrained the neutrino flux using the measured gamma-ray spectrum. Another search by T.-Q. Huang & Z. Li (2022b) used 10 yr of public IceCube track data to search for neutrino emission from the same LHAASO catalog (Z. Cao et al. 2021) with fixed morphology and different spectral models. The IceCube Neutrino Observatory has previously searched for neutrino emission from galactic sources, both individual sources and classes of sources. R. Abbasi et al. (2023a) searched for neutrino emission from LHAASO's first catalog of sources with energy above 100 TeV (Z. Cao et al. 2021) using a fixed spatial extension and a power-law spectrum and 12 yr of IceCube track data. They found no significant emission, neither from single sources nor from stacked catalogs of SNRs and PWNe. Recently, IceCube has detected neutrinos from the galactic plane (R. Abbasi et al. 2023b). The observation was made using a neutrino detection channel, cascades, which has relatively large angular uncertainty. Therefore, IceCube could not distinguish between diffuse emission in the galactic plane and a collection of individual sources. The IceCube collaboration also searched the entire galactic plane and regions near TeV gamma-ray sources using an extended source hypothesis and a power-law spectrum, finding no significant neutrino emission (R. Abbasi et al. 2023c). However, these searches have not directly incorporated gamma-ray data. The simultaneous use of both data sets incorporates more physically motivated spectra and more accurate morphology. In this work, for the first time, we simultaneously use both gamma-ray and neutrino data to improve the sensitivity of the search and provide a direct constraint on the hadronic ratio, i.e., the fraction of gamma-rays originating from hadronic interactions. The improvement in sensitivity of the search comes from the additional 2 yr for data taken with full detector compared to R. Abbasi et al. (2023a) and the modeling of the neutrino emission under the assumption that the gamma-rays and neutrinos originated from the same population of hadrons.

If the gamma-rays and neutrinos originate from hadronic interactions, the spectra of the gamma-rays and neutrinos have a fixed relationship. In the case of Galactic PeVatrons, the proton–proton (pp) interaction is expected to be dominant as compared to the photo-hadronic interactions (M. Ahlers & K. Murase 2014). In the pp interactions, protons interact with nearby material and produce charged and neutral pions. The ratio between the production of charged and neutral pions is about 2:1. Charged pions decay further into three neutrinos and other products, with each resulting neutrino having about a quarter of the energy of the charged pion. The neutral pions decay into two gamma-rays, each with half of the energy of the neutral pion, on average. Therefore, we expect that, for charged and neutral pion decay, the energy of the neutrino produced will be half the energy of the gamma-ray produced on average. On Earth, the observed flux is

$$E_\gamma J_\gamma(E_\gamma) \approx e^{\frac{-d}{\lambda_{\gamma\gamma}}} \frac{1}{3} \sum_{\nu_\alpha} E_\nu J_{\nu_\alpha}(E_\nu), \quad (1)$$

where $J_{\nu_\alpha}(E_\nu)$ is the neutrino differential particle flux with the neutrino flavor α, d is the distance to the source, $\lambda_{\gamma\gamma}$ is the interaction length of the gamma-ray, and $J_\gamma(E_\gamma)$ is the gamma-ray differential particle flux (M. Ahlers & K. Murase 2014). Since we only consider galactic sources, we assume that the absorption of gamma-rays is negligible ($\frac{-d}{\lambda_{\gamma\gamma}} \approx 0$) and the flux

from each neutrino flavor is the same due to oscillations. The relationship between the gamma-ray flux (J_γ) and the muon neutrino flux (J_{ν_μ}) is thus

$$J_{\nu_\mu}(E_{\nu_\mu}) = 2J_\gamma(2E_{\nu_\mu}). \quad (2)$$

Therefore, if the gamma-rays from a galactic source originate from hadronic interactions, the neutrino counterpart should exhibit the same morphology and have the same spectral shape shifted to lower energies. This relationship is used in this work to model and simultaneously fit the gamma-ray and neutrino data.

2. Instruments and Data Sets

2.1. HAWC Gamma-Ray Observatory

The High Altitude Water Cherenkov (HAWC) Observatory is located near Sierra Negra, Mexico, at a latitude of 19°N and an altitude of 4100 m. It has been in continuous operation since 2014 November (A. U. Abeysekara et al. 2023). The observatory consists of 300 Water Cherenkov Detectors (WCDs), covering an area of 22,000 m^2. Each WCD consists of a steel tank 7.3 m in diameter and 5.4 m high, lined with a plastic bladder and filled with purified water. At the bottom of the water tank, three 8-inch photomultiplier tubes (PMTs) are arranged in an equilateral triangle with a side length of 3.2 m, and one 10-inch PMT is in the center (A. U. Abeysekara et al. 2023).

When high-energy gamma-rays interact with the Earth's atmosphere, they create a cascade of particles called an extensive air shower (EAS). When these particles reach the HAWC detector and pass through the water at a speed greater than the speed of light in water, Cherenkov light is induced and collected by the PMTs in the WCDs. HAWC uses the observed Cherenkov emission to reconstruct the properties of the primary gamma-rays.

HAWC divides the detected shower events into a 2D array of analysis bins based on the fraction of triggered PMTs during a shower event and the reconstructed energy of the event (A. U. Abeysekara et al. 2019). The events within an analysis bin are expected to have similar characteristics, including angular resolution, primary gamma-ray energy, and gamma-to-hadron likelihood (signal-to-noise ratio), which allows HAWC to perform a binned likelihood analysis.

In this study, we use 2141 days of HAWC data using the Pass 5 reconstruction (A. Albert et al. 2024). The event-related energy is estimated using the "ground parameter" estimator described in A. U. Abeysekara et al. (2019). This energy estimator uses the charge at a fixed optimal distance from the shower axis to estimate the energy. The data set covers the period from 2015 June 15 to 2021 October 21 with a livetime of more than 90%. The data set contains 29% more data with an improved reconstruction compared to the data set used in the third HAWC catalog (3HWC; A. Albert et al. 2020b).

2.2. The IceCube Neutrino Observatory

The IceCube Neutrino Observatory is a neutrino detector located at the geographic South Pole (M. G. Aartsen et al. 2017). The primary IceCube detector comprises a cubic kilometer array of 5160 digital optical modules (DOMs). These DOMs are arranged along 86 readout and support cables, called strings, embedded in the glacial ice at depths between 1.45 and 2.45 km. Each DOM consists of a 10-inch PMT and its readout electronics and is housed in a pressure-resistant sphere (R. Abbasi et al. 2009). DOMs are designed to detect the Cherenkov light produced by charged particles moving through the ice (R. Abbasi et al. 2010). These particles originate from the charged-current (CC) interactions or neutral-current (NC) interactions of all flavors of neutrinos. IceCube events are typically divided into two categories: track-like events produced by CC interactions of muon neutrinos and cascade-like events from all other CC interactions and NC interactions. The DOMs record the Cherenkov light, allowing events to be classified and event properties, such as the direction of the incident neutrinos and the deposited energy, to be reconstructed (M. G. Aartsen et al. 2014a).

The data set used in this analysis includes 14 yr of IceCube track-like data from 2008 April 6 to 2022 May 23. Track-like data provide a better angular resolution ($\sim 1^\circ$ angular uncertainty for a typical $\sim$TeV neutrino) compared to cascade-like events. This makes track-like events more suited to search for sources with an extension below a few degrees. The data from 2008 April 6 to 2011 May 13 were taken with the partially constructed detector with 40, 59, and 79 strings (IC40, IC59, and IC79), with each configuration spanning approximately one year (M. G. Aartsen et al. 2014b). The remaining data were recorded with the full detector configuration with 86 strings (IC86).

3. Analysis Method

3.1. Source Selection

The 3HWC includes 65 sources with a significance above 5σ based on 1523 days of data (A. Albert et al. 2020b). The 3HWC provides the location and the gamma-ray flux at a pivot energy of 7 TeV for each source in the catalog. The pivot energy E_0 is the energy of normalization of the spectral function, which is specified in terms of E/E_0. If the gamma-ray emission from these sources comes from hadronic interactions, the neutrino flux will be described by the same spectral function with half the pivot energy (3.5 TeV), according to Equation (2). We calculate the IceCube 90% confidence level (CL) sensitivity for a point source with an E^{-2} unbroken power-law spectrum. The sensitivity is defined as the median expected 90% CL upper limit. The sensitivity can be determined using background trials and signal trials. Background trials are done by performing the analysis using simulated data obtained by scrambling real data in R.A. Scrambling data to use as the background does not suffer from systematic uncertainties and therefore is a robust way to generate background trials. Signal trials are generated by scrambling data and adding signal using simulation data. The calculation of sensitivity is based on a maximum likelihood method as used in the IceCube 10 yr search for neutrino sources (M. G. Aartsen et al. 2020b). In this work, we use a new likelihood analysis software component called IceCube Maximum Likelihood Analysis software (i3mla; R. Abbasi et al. 2021) with the Multi-Mission Maximum Likelihood framework (3ML; G. Vianello et al. 2015). Details of i3mla are described in Section 3.4. The likelihood consists of a spatial term and an energy term, as explained in more detail in Appendix A.

We select sources whose predicted neutrino flux from hadronic interactions is larger than the sensitivity of the IceCube E^{-2} point source search. The source selection step is

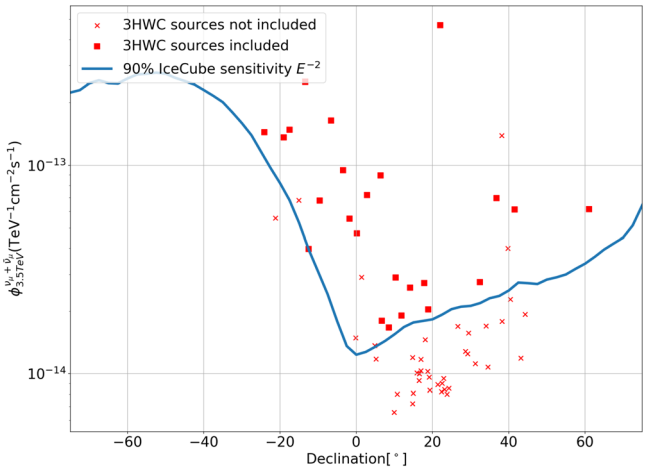

Figure 1. The IceCube E^{-2} time-integrated point source sensitivity as a function of source decl. The x-axis is the decl. in degrees and the y-axis is the differential neutrino flux ($\mathrm{TeV}^{-1}\,\mathrm{cm}^{-2}\,\mathrm{s}^{-1}$) at pivot energy $E_0 = 3.5$ TeV. Each red cross and red square represents the predicted neutrino flux of a 3HWC source assuming all the gamma-rays from the sources originated from proton–proton hadronic interaction. Galactic 3HWC sources (excluding 3HWC secondary sources) with a predicted neutrino flux above the IceCube sensitivity are included in our source list and shown as red squares.

motivated by the trade-off between searching as many possible sources as possible to avoid missing potential sources and avoiding suffering sensitivity loss from the trial factor. The hard E^{-2} spectrum is an optimistic choice made to avoid missing any potential sources in our source selection step, since it is close to the hardest spectrum expected. The sensitivity of the joint search will depend on the best-fit gamma-ray spectrum and spatial extension, and it is different from the E^{-2} point source sensitivity here. The sensitivity of IceCube and the predicted neutrino flux from 3HWC sources are shown in Figure 1. We exclude two extragalactic sources, Markarian 421 and Markarian 501, as this study focuses on galactic sources. We also exclude four sources classified as secondary sources in 3HWC, as these are likely to be statistical fluctuations near bright sources. Our final source list comprises 22 sources from 3HWC. Many of the sources are still unidentified, but some have potential associations with pulsar wind nebulae, supernova remnants, and star-forming regions.

3.2. Model Selection and Fit Using Gamma-Ray Data

To obtain a spatial and spectral model for the joint analysis of the sources, we first fit each gamma-ray source with an updated HAWC data set. We use 2141 days of HAWC ground parameter energy estimator maps with the Pass 5 reconstruction for our model selection procedure. The data set contains 29% more data with an improved reconstruction compared to the data set used in 3HWC. The new reconstruction provides a better angular reconstruction and gamma/hadron separation. We use the 3ML framework (G. Vianello et al. 2015) with the HAWC Accelerated Likelihood (HAL) plugin (A. U. Abeysekara et al. 2021) for our model selection and model fitting. HAL is a Python-based, maximum likelihood software module designed to perform HAWC analysis using a binned likelihood. In conjunction with 3ML, it can perform both standalone HAWC analyses and joint analyses with other experiments. We select the model that best describes the gamma-ray emission based on the log-likelihood (LLH). We use the position in 3HWC as a starting point for our initial fit. First, we use a simple power law and a point source as spectral and spatial hypotheses. The simple power law is parameterized as $\frac{dN_\gamma}{dE_\gamma} = \phi\left(\frac{E_\gamma}{7\ \mathrm{TeV}}\right)^{\alpha}$, where ϕ is the flux normalization and α is the spectral index. The free parameters in this model are the R.A., the decl., the spectral index, and the gamma-ray flux. Second, we test the extended source hypothesis, where we fix the R.A. and decl. of the source to the best-fit values and fit for a Gaussian extension along with the spectral index and flux. We accept the extended source hypothesis if twice the difference between the log-likelihood (2ΔLLH) of the two models (point source hypothesis and extended source hypothesis) is greater than 16, corresponding to 4σ according to the Wilks theorem (S. S. Wilks 1938). Finally, we test the spectrum curvature hypothesis, where we fixed the R.A., decl., and extension (if the source is extended), and we use a log-parabola spectrum to fit the data again. The log-parabola spectrum is parameterized by

$$\frac{dN_\gamma}{dE_\gamma} = \phi \cdot \left(\frac{E_\gamma}{7\ \mathrm{TeV}}\right)^{\alpha-\beta\cdot\log\frac{E_\gamma}{7\ \mathrm{TeV}}}. \tag{3}$$

The free parameters in this model are α, β, and the gamma-ray flux at 7 TeV. We accept the spectral curvature hypothesis if the 2ΔLLH between the spectral curvature hypothesis and the power law hypothesis is greater than 16. Based on the results of these fits, we obtain the final model that contains information about the morphology and spectrum of the source.

3.3. IceCube Likelihood with i3mla

Combining IceCube neutrino data with the HAWC gamma-ray data is a nontrivial task because of the complexity of the instrument response functions and the likelihood calculation. We use a Python-based maximum likelihood module called i3mla (R. Abbasi et al. 2021) for IceCube likelihood calculation. Similar to HAL, i3mla is specifically designed to be compatible with the 3ML framework. i3mla uses instrument response functions (IRFs) to encapsulate the detector properties and performances of the detector determined from Monte Carlo simulations. The IRFs then can be used to calculate the energy likelihood of IceCube. This differs from other IceCube analysis software that precomputes the energy likelihood for an assumed spectrum, e.g., a simple power law, and uses all the Monte Carlo data for the energy likelihood calculation. The new tabulated IRFs method speeds up the likelihood computation process when fitting for an arbitrary spectrum, making it possible to fit any spectral parameters during the model fitting in i3mla.

In this analysis, we use spatial and energy likelihood terms to calculate the likelihood of the model. The signal hypothesis assumes some neutrino emission from the source of interest. The background hypothesis assumes all non-neutrino events and neutrino events originate from atmospheric muons, atmospheric neutrinos, and astrophysical neutrinos that are not associated with the source. We model the IceCube point-spread function (PSF) as a 2D Gaussian, and the angular error of the 2D Gaussian is estimated during the reconstruction. The signal spatial likelihood is the PSF convolved with the morphology of the source, and the signal energy likelihood is calculated using the IRFs and the model spectrum. The background spatial likelihood is estimated from the data by binning the data in reconstructed decl. and creating a spline using the resulting histogram. The background spatial likelihood is a function of decl. only. The background energy likelihood is estimated from

Table 1
Table Summarizing the Model Parameters of the Gamma-Ray and Neutrino Components and Their Relations

Model Parameters	Gamma-Ray Spectrum	Neutrino Spectrum	Relation
R.A.	Fix	Fix	Equal
Decl.	Fix	Fix	Equal
Extension	Fix	Fix	Equal
α	Float	Float	Equal
β	Float	Float	Equal
Pivot energy	Fix	Fix	Neutrino pivot energy = Gamma-ray pivot energy / 2
Flux normalization	Float	Float	Independent

Note. Parameters listed as fix will be fixed during model fitting, and parameters listed as float will be fitted during model fitting.

the data by weighting the simulation using the spectral hypothesis and binning it in reconstructed decl. and energy. The method is conceptually identical to the previous IceCube 10 yr time-integrated point source search in M. G. Aartsen et al. (2020b) and the extended source search in R. Abbasi et al. (2023a, 2023c). A detailed description of the likelihood can be found in Appendix A.

3.4. Joint Fit with Gamma-Rays and Neutrinos

After obtaining a spatial and spectral model for each source, we perform a joint fit with HAWC gamma-ray data and IceCube neutrino data. We keep the location and extension of the model fixed. We add a neutrino component to the model that coincides with the gamma-ray source. We connect the neutrino and gamma-ray emission spectral parameters according to the relation in Equation (2) and allow them to float during the fit. We let the flux normalization of the neutrino and gamma-ray components float independently. Table 1 shows the properties of the model parameters.

To calculate the p-value, we perform a large number of background trials by scrambling the IceCube data in R.A. and building the background test statistic (TS) distribution (M. G. Aartsen et al. 2020c). This is done to avoid any dependence on the simulation when testing for a neutrino source. The calculation of the IceCube component of the likelihood is fast. However, using raw HAWC binned maps for computing the HAWC component of the likelihood is prohibitively computationally expensive for such a large number of trials. Therefore, the HAWC data are fixed during the background scrambling process so that we can precompute the HAWC component of the likelihood. We extract the HAWC likelihood around the best-fit spectral parameters and save it into a table. Since the location and extension are fixed during the fit, we do not extract the likelihood around the spatial parameters. For spectral parameters, we evaluate the HAWC likelihood within $\pm 5\sigma$ of the best-fit spectral shape parameters while maximizing it over the flux normalization.

Since the gamma-ray and neutrino fluxes are floated independently, maximizing the likelihood over the gamma-ray flux normalization leads to a maximum likelihood for

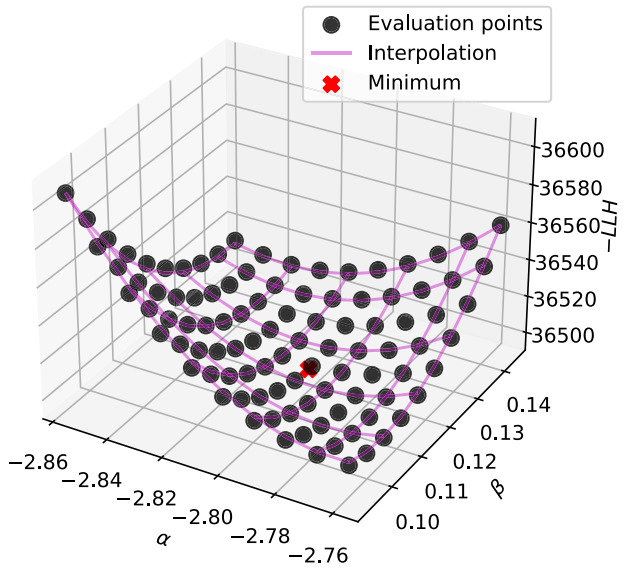

Figure 2. A plot visualizing the HAWC likelihood for an example source. The y-axis is the negative LLH. The negative LLH is evaluated around the best-fit model. For a log-parabola spectrum, we evaluate 50 points within $\pm 5\sigma$ for α and β around the minimum. For a power-law spectrum, we evaluate 300 points for spectral index within $\pm 5\sigma$. The negative log-likelihood was minimized over the gamma-ray flux for each point.

HAWC at the spectral shape parameters in the joint fit. For a log-parabola spectrum, there are two free parameters for the spectral shape (α and β), and we use a 50×50 grid around the best-fit parameters for the likelihood evaluation. For a power-law spectrum, there is only one free parameter for the spectral shape (α) and we evaluate 300 points around the best-fit parameters. We have developed a new custom plugin for 3ML to read the likelihood table and construct a spline. The 3ML plugin then returns the spline values for the likelihood evaluations. This method speeds up the likelihood calculation because the program does not have to calculate the HAWC likelihood for each pixel and each bin during the fitting. Figure 2 shows an example of the likelihood.

The background TS distribution is calculated by generating 50,000 background-only trials. For each background trial, the IceCube data are scrambled in R.A. while keeping the HAWC component of the likelihood unchanged, and the joint analysis is performed. To determine the sensitivity of the joint search for a source with the best-fit parameters, we inject different simulated values of the neutrino flux at the location of the best-fit gamma-ray source with its best-fit extension and spectral shape. The 90% CL sensitivity is the neutrino flux required for the TS to exceed the median of the background-only TS distribution 90% of the time. The 5σ discovery potential is the neutrino flux required for the TS to exceed the 5σ fluctuation of the background-only TS distribution 50% of the time. Figure 3 shows the ratio between the sensitivity and the predicted neutrino flux assuming pp interactions, as well as the ratio between the 5σ discovery potential and the predicted neutrino flux assuming pp interactions.

We derive the pretrial p-value for each source by using the background TS distribution of each source. The pretrial p-value is the percentage of background trials having a TS higher than the TS of the actual search. To correct for the look-elsewhere effect, we create a pretrial p-value distribution by searching for neutrinos from each source using the same background data and picking

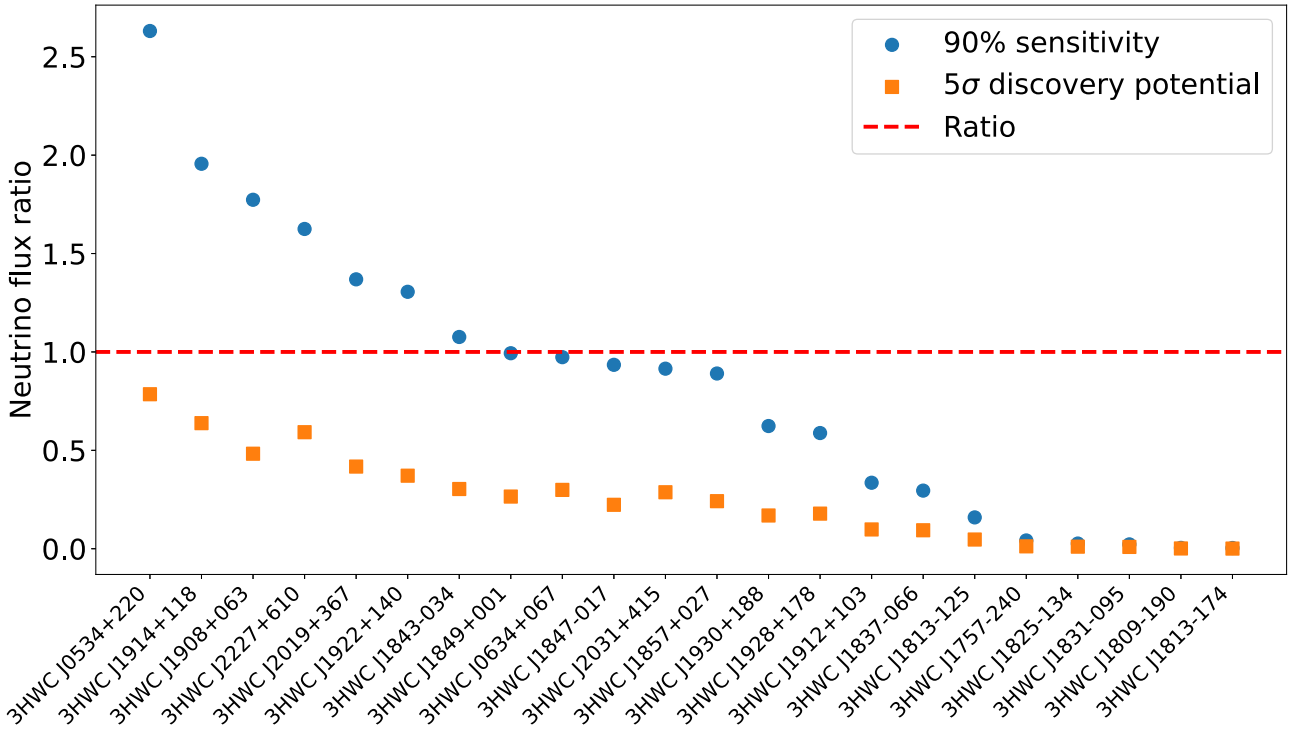

Figure 3. The ratio between the predicted neutrino flux and the sensitivity (blue dot) and 5σ discovery potential (orange rectangle) of the analysis. The sources above the red dashed line are the sources that are likely to be detected by IceCube if they are hadronic sources. The plot is ordered by the sensitivity ratio.

the smallest p-value from the 22 sources in each background trial. The posttrial p-value is the fraction of p-values in the aforementioned distribution that are smaller than the smallest pretrial p-value in the data. With this method, the correlations between different sources can be correctly taken into account.

In addition to searching for individual sources, we perform a binomial test to determine whether a subset of the sources has TS values inconsistent with the background (R. Abbasi et al. 2022a). The test statistic of the binomial test, p_{binomial}, is the minimum probability, over all k, that at least k p-values are at or below the kth smallest p-value observed, p_k:

$$p_{\text{binomial}} = \min_k P_k = \min_k \sum_{m=k}^{N} \binom{N}{m} p_k^m (1 - p_k)^{N-m}. \quad (4)$$

To account for the look-elsewhere effect, we create a distribution of p_{binomial} by performing the binomial test on scrambled data. We compute the posttrial p-value of the binomial test using the p_{binomial} value for data. To calculate the overall posttrial p-value accounting for the trials from doing two searches, we create another p-value distribution by choosing, for each background trial, the smaller of the posttrial p-values from the individual source search and the binomial test. This method takes into account the correlation between the individual source search and the binomial test. We then compare the smaller of the two p-values from data with this distribution to obtain the overall p-value.

4. Results

4.1. HAWC Best-fit Result

First, we present the best-fit results for the gamma-ray emission from the HAWC Pass 5 data alone. Table 2 summarizes the best-fit location, extension, and spectral parameters of each source in our list. In addition, we report the statistical and systematic uncertainty of the spectral fit results. Systematic uncertainties of the HAWC detector include PMT efficiency, charge uncertainty, etc., and are described in A. U. Abeysekara et al. (2019). To evaluate their effect, we perform the model selection using samples simulated with different settings and compare the results with the baseline simulation. The errors of each type of systematic uncertainty are added in quadrature to obtain the total systematic uncertainty, which is given in Table 2. We also reported the 2σ energy range of each source. The upper end of this range is defined such that, if the spectrum is cut off above this energy, the significance of the source drops by 2σ. The corresponding definition is used for the lower end of the sensitivity range. The 2σ threshold is chosen to reasonably claim that HAWC data can probe the quoted energy range at a significance of 2σ or at the $\sim$95% confidence level.

4.2. Joint-fit Result

We performed the joint fit using the best-fit model of HAWC and added a neutrino source as described in Section 3.4. We found no significant neutrino emission. The smallest pretrial p-value from the individual source search is 0.07 for 3HWC J2019+367, which corresponds to a posttrial p-value of 0.21 when accounting for the trials in the individual source search. We performed the binomial test and found no significant neutrino emission from any subset of the 22 sources. The smallest pretrial p-value of the binomial test is 0.09 at $k = 6$ (3HWC J2019+367, 3HWC J2031+415, 3HWC J1912+103, 3HWC J1908+063, 3HWC J1857+027, 3HWC J1928+178) and corresponds to a posttrial p-value of 0.34 when only accounting for trials in the binomial test. Accounting for both the trials from the individual source search and the binomial test, the final posttrial p-value is 0.37. We also computed the 90% neutrino energy range for each source using the best-fit morphology and spectrum. The 90% neutrino energy range is

Table 2
The Best-fit Results from the HAWC Data

Name	R.A. (°)	Decl. (°)	Ext (°)	α	β	F_7 (10^{-14} TeV^{-1} cm^{-2} s^{-1})	Nearest TeVCat	Energy Range (TeV)
3HWC J0534+220	83.64	22.01	PS	$-2.82^{+0.01}_{-0.01}{}^{+0.09}_{-0.03}$	$0.12^{+0.01}_{-0.01}{}^{+0.0}_{-0.05}$	$23.82^{+0.23}_{-0.22}{}^{+0}_{-2.7}$	Crab	0.1–106.1
3HWC J0634+067	98.59	6.66	0.49	$-2.57^{+0.1}_{-0.1}{}^{+0.21}_{-0.0}$	0	$1.35^{+0.43}_{-0.32}{}^{+0}_{-2.6}$	HAWC J0635+070	1.7–53.1
3HWC J1757−240	269.32	−23.86	PS	$-2.58^{+0.26}_{-0.26}{}^{+0.97}_{-0.11}$	0	$1.68^{+1.03}_{-0.66}{}^{+0}_{-1.5}$	HESS J1800−240B	16.9–59.7
3HWC J1809−190	272.42	−19.34	0.23	$-2.09^{+0.15}_{-0.15}{}^{+0.01}_{-0.27}$	$0.23^{+0.07}_{-0.07}{}^{+0.0}_{-0.3}$	$11.69^{+1.11}_{-1.06}{}^{+0}_{-3.1}$	HESS J1809−193	3.0–94.5
3HWC J1813−125	273.4	−12.7	0.27	$-2.6^{+0.08}_{-0.08}{}^{+0.48}_{-0.0}$	0	$2.87^{+0.47}_{-0.44}{}^{+1.0}_{-0}$	HESS J1813−126	2.4–59.6
3HWC J1813−174	273.4	−17.74	0.26	$-1.91^{+0.16}_{-0.15}{}^{+0.54}_{-0.53}$	$0.35^{+0.08}_{-0.08}{}^{+0.31}_{-0.31}$	$13.47^{+1.22}_{-1.07}{}^{+2.5}_{-5.6}$	2HWC J1814−173	3.4–106.0
3HWC J1825−134	276.49	−13.63	0.46	$-2.45^{+0.02}_{-0.02}{}^{+0.1}_{-0.02}$	$0.13^{+0.02}_{-0.02}{}^{+0.0}_{-0.14}$	$41.02^{+1.12}_{-1.12}{}^{+0}_{-8.9}$	2HWC J1825−134	0.5–106.0
3HWC J1831−095	277.85	−9.85	1.14	$-2.59^{+0.03}_{-0.04}{}^{+0.22}_{-0.0}$	$0.14^{+0.02}_{-0.03}{}^{+0.0}_{-0.18}$	$37.37^{+2.08}_{-1.9}{}^{+0}_{-8.4}$	HESS J1831−098	0.4–118.7
3HWC J1837−066	279.38	−6.83	0.65	$-2.69^{+0.02}_{-0.02}{}^{+0.14}_{-0.0}$	$0.1^{+0.01}_{-0.01}{}^{+0.0}_{-0.08}$	$34.52^{+0.89}_{-0.88}{}^{+0}_{-4.8}$	2HWC J1837−065	0.2–133.2
3HWC J1843−034	280.95	−3.39	0.6	$-2.51^{+0.03}_{-0.03}{}^{+0.2}_{-0.0}$	$0.13^{+0.02}_{-0.02}{}^{+0.0}_{-0.21}$	$21.51^{+0.79}_{-0.74}{}^{+0}_{-8.4}$	2HWC J1844−032	0.3–75.0
3HWC J1847−017	282.07	−1.78	0.75	$-2.66^{+0.03}_{-0.03}{}^{+0.28}_{-0.0}$	$0.09^{+0.02}_{-0.02}{}^{+0.0}_{-0.18}$	$17.03^{+0.81}_{-0.76}{}^{+0}_{-2.7}$	HESS J1848−018	0.3–84.0
3HWC J1849+001	282.31	0.02	0.68	$-2.42^{+0.03}_{-0.04}{}^{+0.22}_{-0.0}$	$0.13^{+0.02}_{-0.02}{}^{+0.0}_{-0.24}$	$15.38^{+0.69}_{-0.7}{}^{+0}_{-3.9}$	IGR J18490−0000	0.4–149.8
3HWC J1857+027	284.35	2.82	0.6	$-2.73^{+0.02}_{-0.02}{}^{+0.28}_{-0.0}$	$0.13^{+0.02}_{-0.02}{}^{+0.0}_{-0.18}$	$16.3^{+0.59}_{-0.58}{}^{+0}_{-3.3}$	HESS J1857+026	0.3–133.2
3HWC J1908+063	287.02	6.35	0.57	$-2.44^{+0.02}_{-0.02}{}^{+0.09}_{-0.01}$	$0.09^{+0.01}_{-0.01}{}^{+0.0}_{-0.07}$	$20.02^{+0.52}_{-0.5}{}^{+0}_{-2.6}$	MGRO J1908+06	0.4–168.0
3HWC J1912+103	288.1	10.32	0.52	$-2.83^{+0.05}_{-0.05}{}^{+0.32}_{-0.0}$	$0.14^{+0.04}_{-0.04}{}^{+0.0}_{-0.16}$	$5.79^{+0.47}_{-0.44}{}^{+2.2}_{-5.6}$	HESS J1912+101	0.4–94.4
3HWC J1914+118	288.71	11.79	0.71	$-2.69^{+0.04}_{-0.04}{}^{+0.39}_{-0.0}$	0	$4.09^{+0.59}_{-0.5}{}^{+0}_{-2.6}$	2HWC J1914+117*	0.3–106.0
3HWC J1922+140	290.74	14.06	0.13	$-2.77^{+0.06}_{-0.05}{}^{+0.12}_{-0.0}$	0	$1.37^{+0.17}_{-0.12}{}^{+0.054}_{-0.071}$	W 51	0.2–47.3
3HWC J1928+178	292.13	17.81	0.83	$-2.52^{+0.04}_{-0.04}{}^{+0.18}_{-0.0}$	$0.11^{+0.02}_{-0.03}{}^{+0.0}_{-0.14}$	$9.4^{+0.58}_{-0.54}{}^{+0}_{-1.7}$	2HWC J1928+177	0.6–106.0
3HWC J1930+188	292.56	18.81	0.76	$-2.51^{+0.04}_{-0.04}{}^{+0.12}_{-0.0}$	$0.14^{+0.03}_{-0.03}{}^{+0.0}_{-0.12}$	$9.0^{+0.49}_{-0.48}{}^{+0}_{-2.2}$	SNR G054.1+00.3	0.7–105.9
3HWC J2019+367	304.9	36.77	0.32	$-2.04^{+0.05}_{-0.05}{}^{+0.02}_{-0.13}$	$0.31^{+0.03}_{-0.03}{}^{+0.0}_{-0.22}$	$11.7^{+0.4}_{-0.38}{}^{+0}_{-2.3}$	VER J2019+368	0.9–106.0
3HWC J2031+415	308.01	41.49	0.51	$-2.52^{+0.04}_{-0.04}{}^{+0.26}_{-0.0}$	$0.19^{+0.03}_{-0.03}{}^{+0.0}_{-0.28}$	$12.06^{+0.59}_{-0.56}{}^{+0}_{-3.7}$	TeV J2032+4130	0.5–105.9
3HWC J2227+610	336.82	60.94	PS	$-2.42^{+0.2}_{-0.21}{}^{+0.78}_{-0.27}$	0	$1.53^{+0.68}_{-0.47}{}^{+0.5}_{-1.5}$	Boomerang	16.7–33.5

Notes. The columns from left to right are 3HWC source name, R.A., decl., Gaussian extension (PS indicates a point source), α and β of the log-parabola spectrum ($\beta = 0$ for power-law spectra), the differential gamma-ray flux at 7 TeV, the nearest TeVCat source listed in 3HWC (S. P. Wakely & D. Horan 2008; A. Albert et al. 2020b), and the 2σ energy range. The first uncertainty is statistical and the second is systematics.

the central 90% range of true neutrino energy when injecting signal neutrinos with the source's best-fit gamma-ray morphology and spectrum. IceCube applies a higher energy threshold for neutrino events from the southern sky, due to the containment of atmospheric muons, resulting in a higher energy range for southern sources.

Based on the null result of the joint search, we also calculated the neutrino flux limits at 90% CL for the 22 sources (see Table 3). We account for IceCube systematics by calculating the sensitivity using different Monte Carlo systematic sets and adding the difference to the baseline in quadrature. Appendix B details the effect of IceCube systematics on the flux limit for each source. Table 3 shows the neutrino flux limit for each source. Figure 4 shows, by decl., the neutrino flux limit and the neutrino flux predicted from the best gamma-ray fit assuming all the gamma-ray emission is from hadronic interaction.

Five sources have a lower neutrino 90% CL flux limit than the predicted neutrino flux. In these cases, we conclude that the gamma-ray emission detected in the HAWC energy range cannot completely originate from hadronic interactions. This assumes that the HAWC observed spectrum extends to the IceCube energy range, and it does not account for HAWC spectral uncertainty. If we further assume that the leptonic component shares a similar spectral shape in the TeV energy range, we can constrain the percentage of the gamma-ray flux originating from hadronic interactions. Among these sources, 3HWC J2227+610 was studied by the HAWC collaboration and could be associated with supernova remnant G106.3+2.7. HAWC found a hint of PeV proton acceleration and suggested that 3HWC J2227+610 could be a Galactic PeVatron (A. Albert et al. 2020a). The Crab Nebula (3HWC J0534 +220) is the brightest source in the TeV sky and is the most strongly constrained. However, the Crab Nebula is widely believed to be a leptonic source. A more sensitive neutrino instrument is required to put a relevant constraint, in the ∼1% range, on the hadronic fraction. 3HWC J1922+140 is close to the W 51 region, which contains the star-forming region W51B, the supernova remnant W51C, and a potential PWN,

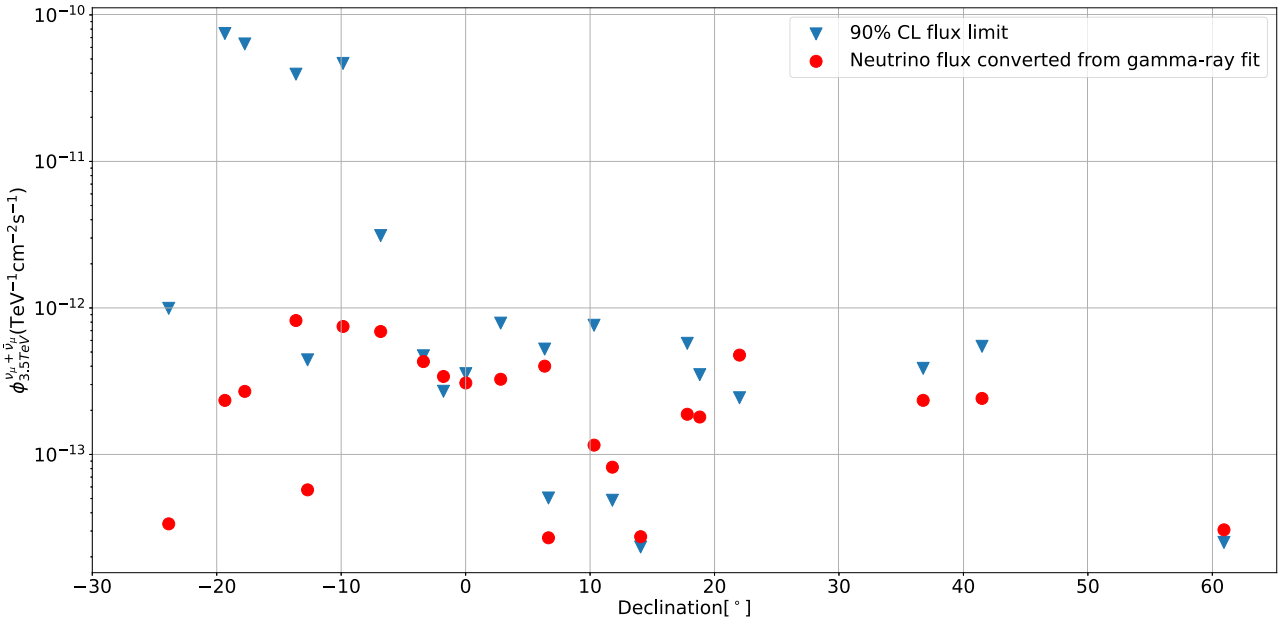

Figure 4. Neutrino 90% CL flux limit from the individual source search. The blue triangles represent the flux limit and the red dots represent the neutrino flux predicted from the gamma-ray best fit assuming all the gamma-ray emission originated from hadronic interaction. Sources that have a predicted neutrino flux higher than the flux limit are the sources for which we can place a hadronic fraction constraint.

Table 3
Neutrino 90% CL Flux Limit at 3.5 TeV from the Individual Source Search

Name	R.A. (°)	Decl. (°)	Extension (°)	*p*-value	Neutrino 90% CL Flux Limit (TeV^{-1} cm^{-2} s^{-1})	Predicted Neutrino Flux (TeV^{-1} cm^{-2} s^{-1})	Energy Range (TeV)
3HWC J0534+220	83.64	22.01	PS	0.36	2.44×10^{-13}	4.74×10^{-13}	0.3–21.6
3HWC J0634+067	98.59	6.66	PS	0.19	5.04×10^{-14}	2.74×10^{-14}	0.4–143.0
3HWC J1757−240	269.32	−23.86	0.10	1	9.94×10^{-13}	3.35×10^{-14}	98.7–6870.0
3HWC J1809−190	272.42	−19.34	0.23	1	7.47×10^{-11}	2.32×10^{-13}	38.7–468.3
3HWC J1813−125	273.40	−12.70	0.27	1	4.42×10^{-13}	5.55×10^{-14}	41.3–3897.3
3HWC J1813−174	273.40	−17.74	0.26	0.7	6.33×10^{-11}	2.72×10^{-13}	9.60–263.5
3HWC J1825−134	276.49	−13.63	0.46	1	3.94×10^{-11}	8.00×10^{-13}	26.2–519.7
3HWC J1831−095	277.85	−9.85	1.14	1	4.71×10^{-11}	7.39×10^{-13}	3.1–229.4
3HWC J1837−066	279.38	−6.83	0.65	1	3.12×10^{-12}	6.91×10^{-13}	0.7–94.1
3HWC J1843−034	280.95	−3.39	0.60	1	4.71×10^{-13}	4.28×10^{-13}	0.7–57.0
3HWC J1847−017	282.07	−1.78	0.75	1	2.70×10^{-13}	3.45×10^{-13}	0.5–49.1
3HWC J1849+001	282.31	0.02	0.68	1	3.56×10^{-13}	3.08×10^{-13}	0.7–56.9
3HWC J1857+027	284.35	2.82	0.60	0.13	7.87×10^{-13}	3.26×10^{-13}	0.4–29.2
3HWC J1908+063	287.02	6.35	0.57	0.1	5.24×10^{-13}	4.00×10^{-13}	0.6–65.1
3HWC J1912+103	288.10	10.32	0.52	0.08	7.61×10^{-13}	1.11×10^{-13}	0.4–24.1
3HWC J1914+118	288.71	11.79	0.71	1	4.87×10^{-14}	7.93×10^{-14}	0.3–73.9
3HWC J1922+140	290.74	14.06	0.13	1	2.33×10^{-14}	2.68×10^{-14}	0.3–51.8
3HWC J1928+178	292.13	17.81	0.83	0.14	5.73×10^{-13}	1.85×10^{-13}	0.5–42.7
3HWC J1930+188	292.56	18.81	0.76	0.1	3.50×10^{-13}	1.78×10^{-13}	0.5–36.6
3HWC J2019+367	304.90	36.77	0.32	0.07	3.87×10^{-13}	2.34×10^{-13}	1.1–34.2
3HWC J2031+415	308.01	41.49	0.51	0.08	5.47×10^{-13}	2.40×10^{-13}	0.5–25.8
3HWC J2227+610	336.82	60.94	PS	1	2.51×10^{-14}	3.11×10^{-14}	0.4–78.4

Notes. The neutrino flux limit is calculated by injecting a flux of neutrino according to the gamma-ray best-fit model's neutrino prediction. The predicted neutrino flux is calculated from the gamma-ray fit result assuming the emission is purely hadronic. The IceCube 90% energy range is the central 90% energy range of the signal neutrinos. The smallest pretrial *p*-value is 0.07, and it corresponds to 0.21 posttrial *p*-value after accounting for trials in the individual source search.

Table 4
Table Showing the Sources That Have a Neutrino 90% CL Flux Limit Lower than the Predicted Neutrino Flux at 3.5 TeV When Assuming the Source Is Hadronic

Name	α	β	Neutrino 90% CL Flux Limit (TeV^{-1} cm^{-2} s^{-1})	p-value	Hadronic Fraction Limit
3HWC J1847−017	−2.66	0.09	2.70×10^{-13}	1	0.79
3HWC J1914+118	−2.69	0	4.87×10^{-14}	1	0.59
3HWC J1922+140	−2.77	0	2.33×10^{-14}	1	0.85
3HWC J0534+220	−2.82	0.12	2.44×10^{-13}	0.36	0.51
3HWC J2227+610	−2.42	0	2.51×10^{-14}	1	0.82

Notes. The p-value is the pretrial p-value from the individual source search, and a p-value of 1 corresponds to a TS of 0 in the search. The hadronic fraction limit is the ratio between the flux limit and the predicted neutrino flux at 3.5 TeV, representing the maximum hadronic fraction—assuming the leptonic emission shares a similar spectral shape.

CXOU J192318.5+140305 (H. Abdalla et al. 2018). 3HWC J1922+140 could be a composite of different astrophysical origins. Table 4 shows the constraints on the hadronic fraction, which range from 51% to 85%.

5. Summary and Discussion

In this paper, we present a new method for performing multimessenger spectral fits with the 3ML software framework (G. Vianello et al. 2015) using HAWC and IceCube data. This is motivated by the predicted neutrino emission by Galactic cosmic-ray accelerators with gamma-ray emission. The new joint-fitting method with gamma-ray data and neutrino data brings improvement in search sensitivity due to more detailed modeling of the neutrino emission under the assumption that the gamma-rays and neutrinos originated from the same population of hadrons. In addition, we could provide a direct constraint on the hadronic ratio in the case of null detection using the emission model derived from the gamma-ray data if the assumption is true. We stress the caveat that a mismodeling of the emission region—for example, due to gamma-rays and neutrinos being produced in different regions of a source—could weaken the constraints presented in this paper.

We used the HAWC data to obtain the best-fit model for the gamma-ray emission. We performed a joint fit using HAWC and IceCube data to search for neutrino emission from potential Galactic cosmic-ray accelerators. No significant neutrino emission was observed. The most significant source from the joint fit is 3HWC J2019+367, with the lowest pretrial p-value of 0.07, corresponding to a posttrial p-value of 0.21. A binomial test for an excess distributed over several sources was performed. The binomial test gave a pretrial p-value of 0.09, obtained for the six most significant sources and corresponding to a posttrial p-value of 0.34. After trial correction for the two searches, the overall posttrial p-value is 0.37. We calculated upper limits at 90% confidence level on the neutrino flux, assuming the spectral form corresponding to the best fit for gamma-rays. We found that five sources have a neutrino flux limit that is lower than the predicted neutrino flux of a purely hadronic source. We conclude that these five sources cannot be purely hadronic and constrain the hadronic fraction of these sources.

We found that, for some of the sources, the HAWC data do not show a 2σ significance for emission above 100 TeV, meaning that the analysis would not warrant the conclusion that those sources are PeVatrons even if neutrinos are detected from the source. In addition, the neutrino 90% energy range for some of the sources does not exceed 50 TeV, meaning the neutrino data would likely not be grounds to establish PeV cosmic-ray acceleration in the case of detection. A more sensitive experiment such as LHAASO could potentially determine the limit on the maximum energy of the source, and neutrino detection could act as evidence of hadronic interactions. In addition, it could provide more PeVatron candidates with better gamma-ray spectrum and morphology measurement. The recently released 1LHAASO catalog contains 43 sources with gamma-ray emission above 100 TeV (Z. Cao et al. 2024b), and a joint search with neutrino data will provide better sensitivity and constraints on their hadronic emission. Next-generation neutrino detectors can improve our understanding of the physical processes of these TeV gamma-ray emitters. The proposed IceCube-Gen2 detector (M. G. Aartsen et al. 2021), with an increased effective area compared to IceCube, is expected to become up to five times more sensitive to galactic neutrino sources. Several neutrino experiments, such as the proposed Pacific Ocean Neutrino Experiment (P-ONE; M. Agostini et al. 2020), Tropical Deep-sea Neutrino Telescope (TRIDENT; Z. P. Ye et al. 2023), KM3NeT (currently under construction; A. Margiotta 2014) and Baikal-GVD (operating and undergoing upgrade) (A. V. Avrorin et al. 2022), are located in the northern hemisphere and have the potential to detect galactic neutrino sources near the Galactic center. The proposed SWGO experiment, which is a ground-based gamma-ray water Cherenkov observatory in the southern hemisphere, would be able to discover more TeV gamma-rays sources in the southern sky and candidates of Galactic PeVatrons (P. Huentemeyer et al. 2019).

Acknowledgments

HAWC: We acknowledge the support from: the US National Science Foundation (NSF); the US Department of Energy Office of High-Energy Physics; the Laboratory Directed Research and Development (LDRD) program of Los Alamos National Laboratory; Consejo Nacional de Ciencia y Tecnología (CONACyT), México, grants 271051, 232656, 260378, 179588, 254964, 258865, 243290, 132197, A1-S-46288, A1-S-22784, CF-2023-I-645, cátedras 873, 1563, 341, 323, Red HAWC, México; DGAPA-UNAM grants IG101323, IN111716-3, IN111419, IA102019, IN106521, IN114924, IN110521 , IN102223; VIEP-BUAP; PIFI 2012, 2013, PROFOCIE 2014, 2015; the University of Wisconsin Alumni Research Foundation; the Institute of Geophysics, Planetary Physics, and Signatures at Los Alamos National Laboratory; Polish Science Centre grant, DEC-2017/27/B/ST9/02272; Coordinación de la Investigación Científica de la

Universidad Michoacana; Royal Society–Newton Advanced Fellowship 180385; Generalitat Valenciana, grant CIDEGENT/2018/034; The Program Management Unit for Human Resources & Institutional Development, Research and Innovation, NXPO (grant number B16F630069); Coordinación General Académica e Innovación (CGAI-UdeG), PRODEP-SEP UDG-CA-499; Institute for Cosmic Ray Research (ICRR), University of Tokyo; National Research Foundation of Korea (RS-2023-00280210). H.F. acknowledges support by NASA under award number 80GSFC21M0002. We also acknowledge the significant contributions over many years of Stefan Westerhoff, Gaurang Yodh, and Arnulfo Zepeda Domínguez, all deceased members of the HAWC collaboration. Thanks to Scott Delay, Luciano Díaz, and Eduardo Murrieta for technical support.

IceCube: The IceCube collaboration acknowledges the significant contributions to this manuscript from Kwok Lung Fan. The authors gratefully acknowledge the support from the following agencies and institutions: USA—U.S. National Science Foundation–Office of Polar Programs, U.S. National Science Foundation-Physics Division, U.S. National Science Foundation–EPSCoR, U.S. National Science Foundation–Office of Advanced Cyberinfrastructure, Wisconsin Alumni Research Foundation, Center for High Throughput Computing (CHTC) at the University of Wisconsin-Madison, Open Science Grid (OSG), Partnership to Advance Throughput Computing (PATh), Advanced Cyberinfrastructure Coordination Ecosystem: Services & Support (ACCESS), Frontera computing project at the Texas Advanced Computing Center, U.S. Department of Energy–National Energy Research Scientific Computing Center, Particle astrophysics research computing center at the University of Maryland, Institute for Cyber-Enabled Research at Michigan State University, Astroparticle physics computational facility at Marquette University, NVIDIA Corporation, and Google Cloud Platform; Belgium—Funds for Scientific Research (FRS-FNRS and FWO), FWO Odysseus and Big Science programmes, and Belgian Federal Science Policy Office (Belspo); Germany—Bundesministerium für Bildung und Forschung (BMBF), Deutsche Forschungsgemeinschaft (DFG), Helmholtz Alliance for Astroparticle Physics (HAP), Initiative and Networking Fund of the Helmholtz Association, Deutsches Elektronen Synchrotron (DESY), and High Performance Computing cluster of the RWTH Aachen; Sweden—Swedish Research Council, Swedish Polar Research Secretariat, Swedish National Infrastructure for Computing (SNIC), and Knut and Alice Wallenberg Foundation; European Union—EGI Advanced Computing for research; Australia—Australian Research Council; Canada—Natural Sciences and Engineering Research Council of Canada, Calcul Québec, Compute Ontario, Canada Foundation for Innovation, WestGrid, and Digital Research Alliance of Canada; Denmark—Villum Fonden, Carlsberg Foundation, and European Commission; New Zealand—Marsden Fund; Japan—Japan Society for Promotion of Science (JSPS) and Institute for Global Prominent Research (IGPR) of Chiba University; Korea—National Research Foundation of Korea (NRF); Switzerland—Swiss National Science Foundation (SNSF).

Appendix A
Likelihood Formalism

HAWC performs a binned likelihood analysis for studying gamma-ray sources. In this analysis, we use the energy binning, the fraction of PMTs hit (*fhit*) binning, and also Healpix Nside = 1024 spatial binning. We calculate the expected background for each bin by applying direct integration using the zenith distribution of all events passing the gamma/hadron cuts. The technique of direct integration has been described in previous HAWC publications (A. U. Abeysekara et al. 2019). The expected excess in every bin is calculated based on the physics model and the detector response of HAWC. The total log-likelihood is the sum of the Poisson log-likelihood of each bin and pixel:

$$\ln \mathcal{L}_{\rm HAWC} = \sum_{j}^{N_{\rm bin}} \sum_{i}^{N_{\rm pixels}} \ln \frac{(b_{ij} + e_{ij} f)^{d_{ij}} e^{-(b_{ij}+e_{ij}f)}}{d_{ij}!}, \tag{A1}$$

where b_{ij} is the expected background at bin j and pixel i, e_{ij} is the expected excess per unit flux given the model at bin j and pixel i, f is the flux, and d_{ij} is the actual count in bin j and pixel i. Index j loops over the energy and *fhit* bin and index i loops over the number of pixels in the region of interest.

For IceCube, we perform an unbinned likelihood analysis. The total likelihood is given by

$$\mathcal{L}_{\rm IceCube} = \prod_{i}^{N} L_i(\boldsymbol{\theta}, \boldsymbol{D_i}) = \prod_{i}^{N} \left(\frac{n_s}{N} S\,(\boldsymbol{\theta}, \boldsymbol{D_i}) + \frac{N - n_s}{N} B(\boldsymbol{D_i}) \right), \tag{A2}$$

where $\boldsymbol{\theta}$ represents the properties of the source hypothesis like location, morphology, and spectrum. L_i is the likelihood of the event i. The parameter vector $\boldsymbol{D_i}$ represents the reconstruction information of the event i, including reconstructed energy, direction, and estimated angular error. N is the total number of events and n_s is the number of signal neutrinos. S and B are the signal probability density function (PDF) and background probability density function, each consisting of a product of a spatial likelihood and an energy likelihood. A detailed description of the IceCube likelihood for extended sources can be found in R. Abbasi et al. (2023a). Since the background likelihood only depends on the reconstructed information of the event and does not depend on the source hypothesis, it is a constant during the fitting process. Therefore, we can divide the likelihood by the likelihood of the background-only hypothesis to get the likelihood ratio that is still a valid likelihood. We rewrite the IceCube log-likelihood to be

$$\ln \mathcal{L}_{\rm IceCube} = \sum_{i}^{N} \ln \left(\frac{n_s}{N} \left(\frac{S(\boldsymbol{D_i}, \boldsymbol{\theta})}{B(\boldsymbol{D_i})} - 1 \right) + 1 \right). \tag{A3}$$

Since HAWC and IceCube measurements are independent, the total log-likelihood for the joint fit is the addition of the HAWC log-likelihood and IceCube log-likelihood:

$$\ln \mathcal{L}_{\rm HAWC} + \ln \mathcal{L}_{\rm IceCube} = \sum_{j}^{N_{\rm bin}} \sum_{i}^{N_{\rm pixels}} \ln \frac{(b_{ij} + e_{ij} f)^{d_{ij}} e^{-(b_{ij}+e_{ij}f)}}{d_{ij}!} + \sum_{i}^{N} \ln \left(\frac{n_s}{N} \left(\frac{S(\boldsymbol{D_i}, \boldsymbol{\theta}}{B(\boldsymbol{D_i})} - 1 \right) + 1 \right). \tag{A4}$$

The combined log-likelihood is then maximized over the free parameters in the model.

Appendix B
IceCube Systematics

In this analysis, we consider the effect of uncertainties on the scattering and absorption of light in the ice, uncertainty in DOM efficiency, and uncertainty in the modeling of ice properties. We consider ±5% uncertainty in absorption and scattering, ±10% in DOM efficiency, and uncertainty in hole ice modeling parameters as described in P. Eller et al. (2023). The method of handling the systematic uncertainties is similar to the one previously used in IceCube's measurement of the diffuse neutrino flux (R. Abbasi et al. 2022b). We use different simulation data sets, each with the value of one parameter changed to account for its systematic uncertainty. The change in sensitivity for the joint analysis as compared to the baseline was calculated for the different sources of systematic uncertainties, and these changes were added in quadrature. Table 5 shows the total systematic uncertainty on the neutrino 90% CL flux limit from each source. The final neutrino flux limit of each source is increased by the total systematic uncertainty and is shown in Table 3.

Table 5
The Total IceCube Systematics for Each Source

Name	Total Systematic Uncertainties
3HWC J0534+220	18%
3HWC J0634+067	25%
3HWC J1757−240	25%
3HWC J1809−190	39%
3HWC J1813−125	27%
3HWC J1813−174	54%
3HWC J1825−134	30%
3HWC J1831−095	40%
3HWC J1837−066	33%
3HWC J1843−034	19%
3HWC J1847−017	21%
3HWC J1849+001	19%
3HWC J1857+027	18%
3HWC J1908+063	18%
3HWC J1912+103	21%
3HWC J1914+118	20%
3HWC J1922+140	14%
3HWC J1928+178	13%
3HWC J1930+188	23%
3HWC J2019+367	14%
3HWC J2031+415	16%
3HWC J2227+610	30%

Note. We add 1 to the numbers and then multiply by the neutrino 90% CL flux limit computed from baseline Monte Carlo to obtain the final neutrino flux limit.

ORCID iDs

H. A. Ayala Solares https://orcid.org/0000-0002-2084-5049
T. Capistrán https://orcid.org/0000-0003-2158-2292
S. Casanova https://orcid.org/0000-0002-6144-9122
U. Cotti https://orcid.org/0000-0002-7607-9582
J. Cotzomi https://orcid.org/0000-0002-1132-871X
E. De la Fuente https://orcid.org/0000-0001-9643-4134
J. C. Díaz-Vélez https://orcid.org/0000-0002-0087-0693
K. Engel https://orcid.org/0000-0001-5737-1820
K. L. Fan https://orcid.org/0000-0002-8246-4751
K. Fang https://orcid.org/0000-0002-5387-8138
J. A. García-González https://orcid.org/0000-0002-4188-5584
F. Garfias https://orcid.org/0000-0003-1122-4168
M. M. González https://orcid.org/0000-0002-5209-5641
J. A. Goodman https://orcid.org/0000-0002-9790-1299
D. Huang https://orcid.org/0000-0002-5447-1786
F. Hueyotl-Zahuantitla https://orcid.org/0000-0002-5527-7141
A. Iriarte https://orcid.org/0000-0001-5811-5167
J. Lee https://orcid.org/0000-0002-2467-5673
H. León Vargas https://orcid.org/0000-0001-5516-4975
G. Luis-Raya https://orcid.org/0000-0003-2810-4867
K. Malone https://orcid.org/0000-0001-8088-400X
J. A. Matthews https://orcid.org/0000-0002-2610-863X
M. Mostafá https://orcid.org/0000-0002-7675-4656
L. Nellen https://orcid.org/0000-0003-1059-8731
M. U. Nisa https://orcid.org/0000-0002-6859-3944
N. Omodei https://orcid.org/0000-0002-5448-7577
Y. Pérez Araujo https://orcid.org/0000-0002-8774-8147
E. G. Pérez-Pérez https://orcid.org/0000-0001-5998-4938
C. D. Rho https://orcid.org/0000-0002-6524-9769
D. Rosa-González https://orcid.org/0000-0003-1327-0838
K. Tollefson https://orcid.org/0000-0001-9725-1479
I. Torres https://orcid.org/0000-0002-1689-3945
S. Yu https://orcid.org/0009-0006-3520-3993
S. Yun-Cárcamo https://orcid.org/0000-0002-9307-0133
R. Abbasi https://orcid.org/0000-0001-6141-4205
M. Ackermann https://orcid.org/0000-0001-8952-588X
S. K. Agarwalla https://orcid.org/0000-0002-9714-8866
J. A. Aguilar https://orcid.org/0000-0003-2252-9514
M. Ahlers https://orcid.org/0000-0003-0709-5631
J. M. Alameddine https://orcid.org/0000-0002-9534-9189
K. Andeen https://orcid.org/0000-0001-9394-0007
C. Argüelles https://orcid.org/0000-0003-4186-4182
S. N. Axani https://orcid.org/0000-0001-8866-3826
X. Bai https://orcid.org/0000-0002-1827-9121
A. Balagopal V. https://orcid.org/0000-0001-5367-8876
S. W. Barwick https://orcid.org/0000-0003-2050-6714
V. Basu https://orcid.org/0000-0002-9528-2009
J. J. Beatty https://orcid.org/0000-0003-0481-4952
J. Becker Tjus https://orcid.org/0000-0002-1748-7367
J. Beise https://orcid.org/0000-0002-7448-4189
C. Bellenghi https://orcid.org/0000-0001-8525-7515
S. BenZvi https://orcid.org/0000-0001-5537-4710
E. Bernardini https://orcid.org/0000-0003-3108-1141
E. Blaufuss https://orcid.org/0000-0001-5450-1757
L. Bloom https://orcid.org/0009-0005-9938-3164
S. Blot https://orcid.org/0000-0003-1089-3001
J. Y. Book Motzkin https://orcid.org/0000-0001-6687-5959
C. Boscolo Meneguolo https://orcid.org/0000-0001-8325-4329

S. Böser https://orcid.org/0000-0002-5918-4890
O. Botner https://orcid.org/0000-0001-8588-7306
J. Böttcher https://orcid.org/0000-0002-3387-4236
B. Brinson https://orcid.org/0000-0001-9128-1159
M. A. Campana https://orcid.org/0000-0003-4162-5739
J. Carpio https://orcid.org/0000-0003-0667-6557
D. Chirkin https://orcid.org/0000-0003-4911-1345
B. A. Clark https://orcid.org/0000-0003-4089-2245
A. Coleman https://orcid.org/0000-0003-1510-1712
J. M. Conrad https://orcid.org/0000-0002-6393-0438
P. Coppin https://orcid.org/0000-0001-6869-1280
P. Correa https://orcid.org/0000-0002-1158-6735
D. F. Cowen https://orcid.org/0000-0003-4738-0787
P. Dave https://orcid.org/0000-0002-3879-5115
C. De Clercq https://orcid.org/0000-0001-5266-7059
J. J. DeLaunay https://orcid.org/0000-0001-5229-1995
D. Delgado https://orcid.org/0000-0002-4306-8828
A. Desai https://orcid.org/0000-0001-7405-9994
P. Desiati https://orcid.org/0000-0001-9768-1858
K. D. de Vries https://orcid.org/0000-0002-9842-4068
G. de Wasseige https://orcid.org/0000-0002-1010-5100
T. DeYoung https://orcid.org/0000-0003-4873-3783
A. Diaz https://orcid.org/0000-0001-7206-8336
H. Dujmovic https://orcid.org/0000-0003-1891-0718
M. A. DuVernois https://orcid.org/0000-0002-2987-9691
P. Eller https://orcid.org/0000-0001-6354-5209
D. Elsässer https://orcid.org/0000-0001-6796-3205
H. Erpenbeck https://orcid.org/0000-0001-6319-2108
A. R. Fazely https://orcid.org/0000-0002-6907-8020
A. Fedynitch https://orcid.org/0000-0003-2837-3477
C. Finley https://orcid.org/0000-0003-3350-390X
L. Fischer https://orcid.org/0000-0002-7645-8048
D. Fox https://orcid.org/0000-0002-3714-672X
A. Franckowiak https://orcid.org/0000-0002-5605-2219
P. Fürst https://orcid.org/0000-0002-7951-8042
E. Ganster https://orcid.org/0000-0003-4393-6944
A. Garcia https://orcid.org/0000-0002-8186-2459
A. Ghadimi https://orcid.org/0000-0002-6350-6485
T. Glüsenkamp https://orcid.org/0000-0002-2268-9297
S. J. Gray https://orcid.org/0000-0003-2907-8306
S. Griffin https://orcid.org/0000-0002-0779-9623
S. Griswold https://orcid.org/0000-0002-7321-7513
K. M. Groth https://orcid.org/0000-0002-1581-9049
P. Gutjahr https://orcid.org/0000-0001-7980-7285
C. Haack https://orcid.org/0000-0003-3932-2448
A. Hallgren https://orcid.org/0000-0001-7751-4489
L. Halve https://orcid.org/0000-0003-2237-6714
F. Halzen https://orcid.org/0000-0001-6224-2417
H. Hamdaoui https://orcid.org/0000-0001-5709-2100
A. Haungs https://orcid.org/0000-0002-9638-7574
K. Helbing https://orcid.org/0000-0003-2072-4172
J. Hellrung https://orcid.org/0009-0006-7300-8961
N. Heyer https://orcid.org/0000-0001-9036-8623
C. Hill https://orcid.org/0000-0003-0647-9174
S. Hori https://orcid.org/0009-0007-2644-5955
M. Hostert https://orcid.org/0000-0002-9584-8877
W. Hou https://orcid.org/0000-0003-3422-7185
T. Huber https://orcid.org/0000-0002-6515-1673
K. Hultqvist https://orcid.org/0000-0003-0602-9472
M. Hünnefeld https://orcid.org/0000-0002-2827-6522
W. Iwakiri https://orcid.org/0000-0002-0207-9010
G. S. Japaridze https://orcid.org/0000-0002-7000-5291
M. Jeong https://orcid.org/0000-0003-2420-6639
M. Jin https://orcid.org/0000-0003-0487-5595
B. J. P. Jones https://orcid.org/0000-0003-3400-8986
D. Kang https://orcid.org/0000-0002-5149-9767
W. Kang https://orcid.org/0000-0003-3980-3778
A. Kappes https://orcid.org/0000-0003-1315-3711
T. Karg https://orcid.org/0000-0003-3251-2126
M. Karl https://orcid.org/0000-0003-2475-8951
A. Karle https://orcid.org/0000-0001-9889-5161
U. Katz https://orcid.org/0000-0002-7063-4418
M. Kauer https://orcid.org/0000-0003-1830-9076
J. L. Kelley https://orcid.org/0000-0002-0846-4542
A. Khatee Zathul https://orcid.org/0000-0002-8735-8579
A. Kheirandish https://orcid.org/0000-0001-7074-0539
J. Kiryluk https://orcid.org/0000-0003-0264-3133
S. R. Klein https://orcid.org/0000-0003-2841-6553
A. Kochocki https://orcid.org/0000-0003-3782-0128
R. Koirala https://orcid.org/0000-0002-7735-7169
H. Kolanoski https://orcid.org/0000-0003-0435-2524
T. Kontrimas https://orcid.org/0000-0001-8585-0933
C. Kopper https://orcid.org/0000-0001-6288-7637
D. J. Koskinen https://orcid.org/0000-0002-0514-5917
P. Koundal https://orcid.org/0000-0002-5917-5230
M. Kovacevich https://orcid.org/0000-0002-5019-5745
M. Kowalski https://orcid.org/0000-0001-8594-8666
J. Krishnamoorthi https://orcid.org/0009-0006-1352-2248
K. Kruiswijk https://orcid.org/0009-0002-9261-0537
A. Kumar https://orcid.org/0000-0002-8367-8401
N. Kurahashi https://orcid.org/0000-0003-1047-8094
N. Lad https://orcid.org/0000-0001-9302-5140
C. Lagunas Gualda https://orcid.org/0000-0002-9040-7191
M. Lamoureux https://orcid.org/0000-0002-8860-5826
M. J. Larson https://orcid.org/0000-0002-6996-1155
F. Lauber https://orcid.org/0000-0001-5648-5930
J. P. Lazar https://orcid.org/0000-0003-0928-5025
J. W. Lee https://orcid.org/0000-0001-5681-4941
K. Leonard DeHolton https://orcid.org/0000-0002-8795-0601
A. Leszczyńska https://orcid.org/0000-0003-0935-6313
J. Liao https://orcid.org/0009-0008-8086-586X
M. Lincetto https://orcid.org/0000-0002-1460-3369
L. Lu https://orcid.org/0000-0003-3175-7770
F. Lucarelli https://orcid.org/0000-0002-9558-8788
W. Luszczak https://orcid.org/0000-0003-3085-0674
Y. Lyu https://orcid.org/0000-0002-2333-4383
J. Madsen https://orcid.org/0000-0003-2415-9959
E. Magnus https://orcid.org/0009-0008-8111-1154
E. Manao https://orcid.org/0009-0002-6197-8574
S. Mancina https://orcid.org/0009-0003-9879-3896
I. C. Mariş https://orcid.org/0000-0002-5771-1124
S. Marka https://orcid.org/0000-0002-3957-1324
Z. Marka https://orcid.org/0000-0003-1306-5260
R. Maruyama https://orcid.org/0000-0003-2794-512X
F. Mayhew https://orcid.org/0000-0001-7609-403X
F. McNally https://orcid.org/0000-0002-0785-2244
K. Meagher https://orcid.org/0000-0003-3967-1533
M. Meier https://orcid.org/0000-0002-9483-9450
L. Merten https://orcid.org/0000-0003-1332-9895
T. Montaruli https://orcid.org/0000-0001-5014-2152
R. W. Moore https://orcid.org/0000-0003-4160-4700
M. Moulai https://orcid.org/0000-0001-7909-5812
T. Mukherjee https://orcid.org/0000-0002-0962-4878

R. Naab https://orcid.org/0000-0003-2512-466X
R. Nagai https://orcid.org/0000-0001-7503-2777
J. Necker https://orcid.org/0000-0003-0280-7484
L. Neste https://orcid.org/0000-0002-4829-3469
H. Niederhausen https://orcid.org/0000-0002-9566-4904
K. Noda https://orcid.org/0000-0003-1397-6478
A. Obertacke Pollmann https://orcid.org/0000-0002-2492-043X
V. O'Dell https://orcid.org/0000-0003-0903-543X
B. Oeyen https://orcid.org/0000-0003-2940-3164
E. O'Sullivan https://orcid.org/0000-0003-1882-8802
H. Pandya https://orcid.org/0000-0002-6138-4808
N. Park https://orcid.org/0000-0002-4282-736X
E. N. Paudel https://orcid.org/0000-0001-9276-7994
L. Paul https://orcid.org/0000-0003-4007-2829
C. Pérez de los Heros https://orcid.org/0000-0002-2084-5866
S. Philippen https://orcid.org/0000-0002-0276-0092
A. Pizzuto https://orcid.org/0000-0002-8466-8168
M. Plum https://orcid.org/0000-0001-8691-242X
C. Raab https://orcid.org/0000-0001-9921-2668
A. Rehman https://orcid.org/0000-0001-7616-5790
E. Resconi https://orcid.org/0000-0003-0705-2770
W. Rhode https://orcid.org/0000-0003-2636-5000
B. Riedel https://orcid.org/0000-0002-9524-8943
M. Rongen https://orcid.org/0000-0002-7057-1007
A. Rosted https://orcid.org/0000-0003-2410-400X
C. Rott https://orcid.org/0000-0002-6958-6033
T. Ruhe https://orcid.org/0000-0002-4080-9563
I. Safa https://orcid.org/0000-0001-8737-6825
A. Sandrock https://orcid.org/0000-0002-6779-1172
M. Santander https://orcid.org/0000-0001-7297-8217
S. Sarkar https://orcid.org/0000-0002-1206-4330
S. Sarkar https://orcid.org/0000-0002-3542-858X
H. Schieler https://orcid.org/0000-0002-2637-4778
S. Schindler https://orcid.org/0000-0001-5507-8890
F. Schlüter https://orcid.org/0000-0002-5545-4363
J. Schneider https://orcid.org/0000-0001-7752-5700
F. G. Schröder https://orcid.org/0000-0001-8495-7210
L. Schumacher https://orcid.org/0000-0001-8945-6722
S. Sclafani https://orcid.org/0000-0001-9446-1219
M. Seikh https://orcid.org/0000-0002-4464-7354
S. Seunarine https://orcid.org/0000-0003-3272-6896
P. Sevle Myhr https://orcid.org/0009-0005-9103-4410
N. Shimizu https://orcid.org/0000-0001-6857-1772
M. Silva https://orcid.org/0000-0001-6940-8184
B. Skrzypek https://orcid.org/0000-0002-0910-1057
B. Smithers https://orcid.org/0000-0003-1273-985X
D. Soldin https://orcid.org/0000-0003-3005-7879
P. Soldin https://orcid.org/0000-0003-1761-2495
G. Sommani https://orcid.org/0000-0002-0094-826X
G. M. Spiczak https://orcid.org/0000-0002-0030-0519
C. Spiering https://orcid.org/0000-0001-7372-0074
T. Stezelberger https://orcid.org/0000-0003-2676-9574
T. Stuttard https://orcid.org/0000-0001-7944-279X
G. W. Sullivan https://orcid.org/0000-0002-2585-2352
I. Taboada https://orcid.org/0000-0003-3509-3457
S. Ter-Antonyan https://orcid.org/0000-0002-5788-1369
W. G. Thompson https://orcid.org/0000-0003-2988-7998
J. Thwaites https://orcid.org/0000-0001-9179-3760
S. Toscano https://orcid.org/0000-0002-1860-2240
M. A. Unland Elorrieta https://orcid.org/0000-0002-6124-3255
A. K. Upadhyay https://orcid.org/0000-0003-1957-2626
N. Valtonen-Mattila https://orcid.org/0000-0002-1830-098X
J. Vandenbroucke https://orcid.org/0000-0002-9867-6548
N. van Eijndhoven https://orcid.org/0000-0001-5558-3328
J. van Santen https://orcid.org/0000-0002-2412-9728
S. Verpoest https://orcid.org/0000-0002-3031-3206
A. Wang https://orcid.org/0009-0006-9420-2667
C. Weaver https://orcid.org/0000-0003-2385-2559
C. Wendt https://orcid.org/0000-0001-8076-8877
N. Whitehorn https://orcid.org/0000-0002-3157-0407
C. H. Wiebusch https://orcid.org/0000-0002-6418-3008
L. Witthaus https://orcid.org/0009-0000-0666-3671
M. Wolf https://orcid.org/0000-0001-9991-3923
S. Yoshida https://orcid.org/0000-0003-2480-5105
S. Yu https://orcid.org/0000-0003-4811-9863
T. Yuan https://orcid.org/0000-0002-7041-5872

References

Aartsen, M. G., Abbasi, R., Ackermann, M., et al. 2014a, JInst, 9, P03009
Aartsen, M. G., Abbasi, R., Ackermann, M., et al. 2020a, PhRvD, 102, 122001
Aartsen, M. G., Abbasi, R., Ackermann, M., et al. 2021, JPhG, 48, 060501
Aartsen, M. G., Ackermann, M., Adams, J., et al. 2014b, ApJ, 796, 109
Aartsen, M. G., Ackermann, M., Adams, J., et al. 2017, JInst, 12, P03012
Aartsen, M. G., Ackermann, M., Adams, J., et al. 2020b, PhRvL, 124, 051103
Aartsen, M. G., Ackermann, M., Adams, J., et al. 2020c, PhRvL, 124, 051103
Abbasi, R., Abdou, Y., Abu-Zayyad, T., et al. 2010, NIM A, 618, 139
Abbasi, R., Ackermann, M., Adams, J., et al. 2009, NIM A, 601, 294
Abbasi, R., Ackermann, M., Adams, J., et al. 2021, ICRC (Berlin), 37, 1098
Abbasi, R., Ackermann, M., Adams, J., et al. 2022a, ApJ, 939, 116
Abbasi, R., Ackermann, M., Adams, J., et al. 2022b, ApJ, 928, 50
Abbasi, R., Ackermann, M., Adams, J., et al. 2023a, ApJL, 945, L8
Abbasi, R., Ackermann, M., Adams, J., et al. 2023b, Sci, 380, 1338
Abbasi, R., Ackermann, M., Adams, J., et al. 2023c, ApJ, 956, 20
Abbasi, R. U., Abe, M., Abu-Zayyad, T., et al. 2018, ApJ, 865, 74
Abdalla, H., Abramowski, A., Aharonian, F., et al. 2018, A&A, 612, A1
Abeysekara, A. U., Albert, A., Alfaro, R., et al. 2019, ApJ, 881, 134
Abeysekara, A. U., Albert, A., Alfaro, R., et al. 2023, NIMPA, 1052, 168253
Abeysekara, A. U., Albert, A., Alfaro, R. J., et al. 2021, ICRC (Berlin), 395, 828
Abramowski, A., Aharonian, F., Benkhali, F. A., et al. 2016, Natur, 531, 476
Agostini, M., Böhmer, M., Bosma, J., et al. 2020, NatAs, 4, 913
Ahlers, M., & Murase, K. 2014, PhRvD, 90, 023010
Albert, A., Alfaro, R., Alvarez, C., et al. 2020a, ApJL, 896, L29
Albert, A., Alfaro, R., Alvarez, C., et al. 2020b, ApJ, 905, 76
Albert, A., Alfaro, R., Alvarez, C., et al. 2021, ApJL, 907, L30
Albert, A., Alfaro, R., Alvarez, C., et al. 2022, ApJ, 928, 116
Albert, A., Alfaro, R., Alvarez, C., et al. 2024, ApJ, 972, 144
Amenomori, M., Bao, Y. W., Bi, X. J., et al. 2021, PhRvL, 126, 141101
Amenomori, M., Bi, X. J., Chen, D., et al. 2008, ApJ, 678, 1165
Avrorin, A. V., Avrorin, A. D., Ayinutdinov, V. M., et al. 2022, JETP, 134, 399
Bell, A. R., Schure, K. M., Reville, B., & Giacinti, G. 2013, MNRAS, 431, 415
Blandford, R. D., & Ostriker, J. P. 1978, ApJL, 221, L29
Bykov, A. M., Marcowith, A., Amato, E., et al. 2020, SSRv, 216, 42
Cao, Z., Aharonian, F., An, Q., et al. 2024b, ApJS, 271, 25
Cao, Z., Aharonian, F., Axikegu, et al. 2024a, PhRvL, 132, 131002
Cao, Z., Aharonian, F. A., An, Q., et al. 2021, Natur, 594, 33
de Oña Wilhelmi, E., López-Coto, R., Aharonian, F., et al. 2024, NatAs, 8, 425
Di Palma, I., Guetta, D., & Amato, E. 2017, ApJ, 836, 159
Eller, P., Rongen, M., Abbasi, R., et al. 2023, ICRC (Nagoya), 38, 1034
Gabici, S., & Aharonian, F. A. 2007, ApJL, 665, L131
Glasmacher, M. A. K., Catanese, M. A., Chantell, M. C., et al. 1999, APh, 12, 1
Hess, V. F. 1912, Phys. Z., 13, 1084
Hinton, J. A., & Hofmann, W. 2009, ARA&A, 47, 523
Huang, T.-Q., & Li, Z. 2022a, ApJ, 925, 85
Huang, T.-Q., & Li, Z. 2022b, MNRAS, 514, 852
Huentemeyer, P., BenZvi, S., Dingus, B., et al. 2019, BAAS, 51, 109
Klein, O., & Nishina, T. 1929, ZPhy, 52, 853
LHAASO Collaboration 2024, SciBu, 69, 449
Margiotta, A. 2014, NIMPA, 766, 83
Nagano, M., Hara, T., Hatano, Y., et al. 1984, JPhG, 10, 1295
Vianello, G., Lauer, R. J., Younk, P., et al. 2015, ICRC (The Hague), 34, 1042
Wakely, S. P., & Horan, D. 2008, ICRC (Mérida), 3, 1341
Wilks, S. S. 1938, Ann. Math. Stat., 9, 60
Ye, Z. P., Hu, F., Tian, W., et al. 2023, NatAs, 7, 1497